NATIONAL ADVISORY COMMITTEE FOR AERONAUTICS

TECHNICAL NOTE

No. 1074

TESTS OF A FULL-SCALE HORIZONTAL TAIL SURFACE IN THE LANGLEY 16-FOOT HIGH-SPEED TUNNEL

By Carl F. Schueller, Peter F. Korycinski and H. Kurt Strass

Langley Memorial Aeronautical Laboratory
Langley Field, Va.

Washington
May 1946

NATIONAL ADVISORY COMMITTEE FOR AERONAUTICS

TECHNICAL NOTE No. 1074

TESTS OF A FULL-SCALE HORIZONTAL TAIL SURFACE IN THE LANGLEY 16-FOOT HIGH-SPEED TUNNEL

By Carl F. Schueller, Peter F. Korycinski and H. Kurt Strass

SUMMARY

Tests to determine the aerodynamic characteristics of a full-scale semispan horizontal tail surface of a fighter-type airplane have been conducted in the Langley 16-foot high-speed tunnel. The tests were carried to a maximum Mach number of 0.7 except for model configurations for which the maximum allowable loads were reached at lower speeds. The results presented show the effects of elevator nose shape, elevator trailing-edge angle, and trailing-edge strips on the aerodynamic characteristics of the model. Results are also given for a few measurements of the external and internal elevator pressures and the extent of laminar flow on the stabilizer.

Increasing the Mach number from 0.2 to 0.7 resulted in a marked increase (-0.0015 to -0.0032) in the rate of change of hinge-moment coefficient with elevator deflection, a small increase (0.0025 to 0.0027) in the rate of change of hinge-moment coefficient with angle of attack and an appreciable loss (0.51 to 0.34) in elevator effectiveness.

The incremental changes in elevator hinge-moment characteristics due to modifying the elevator nose contour were of about the same magnitude as would be predicted by the use of recently published methods.

INTRODUCTION

Past experience has shown that surface irregularities and deflections have detrimental effects on the aerodynamic characteristics of horizontal tail surfaces, particularly at high speeds. Accurate estimates of the characteristics of tail surfaces for high-speed airplanes therefore require tests of full-scale models which are reproductions of the tail surface to be used on the airplanes. The model used in these tests was built by conventional manufacturing methods and was for use on an experimental airplane after completion of the wind-tunnel investigation.

The original metal-covered elevator was tested through a range of Mach numbers of 0.2 to 0.7 to determine the aerodynamic characteristics. A few tests were also made to determine the extent of laminar flow, the external and internal elevator pressures, and the effect on the aerodynamic characteristics of trailing-edge strips and of lowering the elevator with respect to the stabilizer.

Several profile modifications of a full-scale wooden elevator were tested at low speed to obtain the effect of nose shape and trailing-edge angle modifications on the elevator characteristics.

COEFFICIENTS AND SYMBOLS

C_D drag coefficient (D/qS)

C_h hinge-moment coefficient $\left(H/q\bar{c}_e^{\,2}b_e\right)$

C_L lift coefficient (L/qS)

C_m pitching-moment coefficient $\left(\frac{M_{c/4}}{qS}\right)$

where

D	drag of horizontal semispan tail surface
H	hinge moment of elevator
L	lift of horizontal semispan tail surface
$M_{c/4}$	pitching moment about quarter-chord point of mean aerodynamic chord
b	span, inches
c	chord of horizontal tail, inches
$\bar{c}_e$	root-mean-square of elevator chord behind hinge line, inches
q	dynamic pressure $\left(\frac{1}{2}\rho V^2\right)$
ρ	density, slugs per cubic foot
V	velocity, feet per second
S	total area, square feet

and

P	pressure coefficient $\left(\frac{p - p_o}{q_o}\right)$
p	static pressure at any point
R	Reynolds number
M	Mach number
α	angle of attack of stabilizer
δ	angle of elevator chord with respect to stabilizer chord (trailing edge down is positive)
ϕ	included angle at elevator trailing edge

and

$$\left(\frac{\partial \alpha}{\partial \delta}\right)_{C_L} = \frac{C_{L_\delta}}{C_{L_\alpha}}$$

$$C_{L_\alpha} = \left(\frac{\partial C_L}{\partial \alpha}\right)_\delta$$

$$C_{L_\delta} = \left(\frac{\partial C_L}{\partial \delta}\right)_\alpha$$

$$C_{h_\alpha} = \left(\frac{\partial C_h}{\partial \alpha}\right)_\delta$$

$$C_{h_\delta} = \left(\frac{\partial C_h}{\partial \delta}\right)_\alpha$$

$$C_{m_\alpha} = \left(\frac{\partial C_m}{\partial \alpha}\right)_\delta$$

$$C_{m_\delta} = \left(\frac{\partial C_m}{\partial \delta}\right)_\alpha$$

$$\left(\frac{\partial C_m}{\partial C_L}\right)_\alpha = \frac{C_{m_\alpha}}{C_{L_\alpha}}$$

$$\left(\frac{\partial C_m}{\partial C_L}\right)_\delta = \frac{C_{m_\delta}}{C_{L_\delta}}$$

The subscripts outside the parentheses represent the factors held constant in the determination of the parameters.

Subscripts:

e elevator

i internal

o free stream

b balance

DESCRIPTION OF MODEL

The model was a full-scale semispan horizontal tail surface of a fighter-type airplane. The airfoil was made according to the NACA 66-009 profile, modified to have a straight contour beyond the 72-percent-chord station. The physical characteristics of the model are given in table I and figure 1.

Stabilizer.- The stabilizer was of metal construction and metal covered. (See fig. 2.) All rivets were flush and the surface had been filled, rubbed with abrasive cloth, and waxed to increase the surface smoothness; however, considerable surface waviness existed. The gap between the elevator and stabilizer was approximately 1/4 inch and was constant for all elevator angles. In order to reduce undesirable air flow through the elevator hinge pockets, the model included cover plates, which were attached to the top and bottom of each stabilizer hinge bracket.

Elevators.- The chordwise and spanwise dimensions of all the elevators tested were equal. The hinge line was located at 72.0 percent of the chord of the horizontal tail and the overhang was 48 percent of the elevator chord $\left(\frac{c_b}{c_e} = 0.48\right)$. No trim tab is used on the elevator of this airplane because the angle of incidence of the stabilizer is adjustable in flight.

The metal elevator was of aluminum construction with no vent or drain holes. The nose shape was semi-elliptical, and the contour was a straight taper behind the hinge line, resulting in a trailing-edge angle of approximately 13°.

Elevators 1, 2, 3, and 4 were constructed of spruce and incorporated systematic modifications to the elevator profile (fig. 3). Elevator 1 had a blunt nose and straight taper behind the hinge line ($\phi = 13°$). Elevator 2 had a blunt nose and a cusped contour behind the

hinge line ($\phi = 7^\circ$). Elevator 3 had a modified blunt nose and a cusped contour behind the hinge line ($\phi = 7^\circ$). Elevator 4 had a semielliptical nose, of the same contour as the metal-covered elevator, and a cusped contour behind the hinge line ($\phi = 7^\circ$). The coordinates of these elevators are given in table II.

Examination of the stabilizer and metal elevator showed that the center line of hinge-bearing in the stabilizer brackets was approximately three thirty-seconds of an inch above the chord line. On the other hand the hinge pins for the metal elevator were found to be slightly above the chord line. As a result of these structural irregularities, the upper surface of the elevator projected approximately one-sixteenth of an inch above the contour of the stabilizer for neutral elevator. The effect of these structural irregularities and the modifications made to compensate for them will be discussed later.

APPARATUS AND METHODS

Model installation.- Inasmuch as a semispan model was used, it was necessary to locate the center line of the horizontal tail surface in the plane of the tunnel-wall flat to produce air-flow conditions more closely simulating those of flight. (See figs. 1 and 2.) Labyrinth-type seals were used where the model support went through the tunnel-wall flat to reduce to a minimum the leakage of air from the test chamber to the tunnel.

Hinge-moment measurement.- The elevator control tube was extended so that it passed through the tunnel flat and two self-alining bearings mounted on the tunnel balance frame. The elevator hinge moment was transferred through the elevator torque tube to a 6-inch crank and then through a jackscrew to the platform of a scale. The jackscrew was also used to vary the elevator angle. The platform scale was attached rigidly to the tunnel balance frame and, since all other related parts were also attached to the tunnel balance frame, there was no possibility of the hinge-moment measurements interfering with the measurements of lift, drag, and pitching moment. All force and moment data were recorded simultaneously.

Elevator angle measurement.- An autosyn was used to measure the elevator angle. The transmitter was attached rigidly to the stabilizer at the inboard hinge cut-out. A small pinion gear on the transmitter shaft was driven by a large gear sector, which was rigidly attached to the root of the elevator. Thus, any elevator deflection was multiplied by the gear ratio (approximately 12:1) and transmitted electrically to the receiver. A calibrated dial attached to the receiver provided a continuous visual indication of the elevator angle. A templet was used to check the zero reading of the autosyn indicator. This system measured the elevator root angle within ±0.1°.

Angle-of-attack measurement.- An inclinometer located on a reference surface of the model support system was used to measure the angle of attack of the stabilizer. The measurement of the root angle of the stabilizer is believed to be accurate within ±0.05°.

Pressure measurements.- Pressure measurements over the nose and top surface of the metal-covered elevator were made by the use of a pressure belt (0.090-inch-diameter tubes) located approximately 47 inches from the center line of the airplane (station 47). External pressures were also measured behind the middle hinge pocket on the top surface of the elevator by means of a small pressure belt. These pressure belts are believed to have no important effect on the pressure distributions.

The internal pressure of the elevator was measured by open-end tubes located in two elevator panels. One tube was located near the inboard end of the elevator (station 30) and the other in the panel adjacent to and on the inboard side of the middle hinge pocket (station 47).

Trailing-edge strips.- Strips of $\frac{1}{8}$-inch- or $\frac{1}{16}$-inch-diameter tubing were attached to both surfaces of the metal elevator at the trailing edge. The method of attaching the tubing to the elevator is shown in figure 4. Strips that were full span, half span, and quarter span in length were tested. The length of the trailing-edge strips was varied by cutting equal lengths from the root and tip ends of the strips. (See fig. 4.)

Transition strips.- The extent of laminar flow over the stabilizer, with metal elevator, was determined by

fixing the transition with $\frac{1}{2}$-inch-wide strips of carborundum on the top surface of the stabilizer at constant percentage of chord stations. Shellac was first applied to the surface as a spanwise strip on which No. 60 powdered carborundum was evenly distributed. Upon completion of the tests with this transition strip, it was removed and the process was repeated at a more forward station. At the 5-percent-chord station tests were made with the strip on the top surface and also with strips on both the top and bottom surfaces.

TESTS

Test data for the metal elevator were generally obtained for angles of attack of -3°, 0°, 3°, 6°, and 9°; elevator deflections of -13°, -8°, -4°, -1°, 0°, 2°, 5°, 9°, and 14°; and M = 0.20, 0.35, 0.45, 0.50, 0.55, 0.60, 0.65, and 0.70 with the original hinge position. The possible combinations of these variables were limited by the maximum allowable load on the model. A few tests also were made with the stabilizer hinge brackets lowered 3/32 inch.

The wooden elevators were tested only at moderate speeds and a small range of angle of attack and elevator angles. Tests to determine the effect of trailing-edge angle (elevators 1 and 2) were made with the original hinge location. Tests to determine the effects of nose shape (elevators 2, 3, and 4) were made with the stabilizer hinge bracket lowered 3/32 inch. Tests of elevator profile modifications, trailing-edge strips, and transition strips included only limited combinations of angle of attack, elevator angle, and speed, usually $\alpha = -3°$ to 3°, $\delta = -8°$ to 9°, and M = 0.35.

REDUCTION OF DATA

The data presented in this report have been corrected for tunnel-wall effects by the use of the reflection-plane theory given in reference 1. The projected frontal area of the model was such a small part of the tunnel area that tunnel-constriction corrections were negligible. Also, corrections to pitching moment due to model deflection and balance-frame deflection were found to be

negligible. The corrected data were cross-plotted and the values at selected angles of attack and elevator angles were then plotted against Mach number. The average dynamic pressures and average Reynolds numbers corresponding to the test Mach numbers are shown in figure 5. The Reynolds number is based on the calculated mean aerodynamic chord of 4.27 feet. The results herein are generally plotted against Mach number rather than velocity or dynamic pressure because Mach number is considered to be the dominating variable. The effects shown in these plots, however, include effects due to distortion of the model under load and are not entirely compressibility effects.

Tests were made with approximately a $\frac{1}{4}$-inch gap around the model support at the tunnel flat, with this gap reduced to a minimum by the use of a labyrinth seal, and with the gap completely sealed with flexible tape. These tests indicated that corrections to the aerodynamic coefficients due to air leakage from the test chamber to the tunnel for the various leak conditions tested were negligible for this setup. All tests were made with the labyrinth-type seal around the model end gap.

RESULTS AND DISCUSSION

Basic Data with Metal Elevator

Effect of angle of attack.- The variation of the aerodynamic coefficients C_L, C_D, and C_m over a wide range of angle of attack at low speed with the metal elevator is shown in figure 6 for $\delta = -0.5°$ and $10.6°$. The low value of maximum C_L obtained prompted a tuft study to determine the origin and progress of the stall. At an angle of attack of 11° a local area of separated flow appeared near the leading edge, centered about 1 foot in from the stabilizer tip and extending over about 1 foot of the span. As the angle of attack was increased, the separation spread backward along the chord and inboard toward the stabilizer root.

Effect of Mach number.- The variation of the aerodynamic characteristics of the metal elevator with Mach

number is shown in figure 7 for $\alpha = -3^\circ$, 0°, 3°, 6°, and 9° and a maximum test range of $\delta = 14^\circ$ to -13°. The increase in C_D with Mach number shown in this figure does not indicate that the critical speed of the tail surface was attained in these tests. The pitching-moment and lift coefficients would be expected, from Glauert's theory, to increase approximately according to the factor $\left(1 - M^2\right)^{-1/2}$; however, figure 7 does not show an increase of this order of magnitude. In fact, for some model configurations at small values of α and large values of δ, the lift coefficients decrease with increasing Mach number, and this decrease is believed to result from twist of the stabilizer when the lift was obtained by deflecting the elevator. The elevator hinge-moment coefficient generally increased with increasing Mach number for $\delta = 9^\circ$ to -8°. This increase was much more rapid than the increase obtained by the use of Glauert's factor $\left(1 - M^2\right)^{-1/2}$. The failure of the test data to increase according to Glauert's factor is not unexpected since this theory does not take into account the effects of boundary layer and structural deformations. At Mach numbers beyond the test range some changes in all coefficients are likely to occur.

Aerodynamic Parameters of Metal Elevator

Lift.- The variation of the lift parameters C_{L_α} and C_{L_δ} of the metal elevator with Mach number is shown in figure 8. The increase of the parameter C_{L_α} with Mach number is less than would be predicted by the use of Glauert's factor and no critical condition is apparent up to a Mach number of 0.70. The gradual decrease of C_{L_δ} with Mach number is an undesirable characteristic and is believed to be due to the gap (0.005c) between the stabilizer and elevator leading edge and partly to the elevator twist. Should the value of C_{L_δ} be used as an indication of elevator effectiveness, figure 8(a) would indicate that the loss in elevator effectiveness is small as the airspeed is increased; however, the ratio $\frac{C_{L_\delta}}{C_{L_\alpha}} = \frac{\partial \alpha}{\partial \delta}$ is usually used as a criterion of elevator effectiveness. The variation of $\partial\alpha/\partial\delta$ with Mach number as shown in figure 8(b) indicates

that the elevator effectiveness decreased from 0.51 at $M = 0.20$ to 0.34 at $M = 0.70$. Since C_{L_α} and C_{L_δ} would be expected to increase with speed and C_{L_δ} actually decreases with speed, the loss of elevator effectiveness with increasing speed is ascribed to the decrease in C_{L_δ}. As mentioned previously, the decrease in C_{L_δ} with increasing speed is believed to result primarily from the gap between the rear part of the stabilizer and the elevator leading edge. This impression is further substantiated by a comparison of the results of tests of another full-scale tail surface at high speeds (reference 2) with the present model. The only important difference between the two horizontal tail surfaces as regards the change in C_{L_δ} with speed is the use of an elevator seal on the model of reference 2. Any differences in the variation of C_{L_δ} with speed for the two models must therefore be an effect of the elevator-gap configuration. In figure 24(a) of reference 2, the value of C_{L_δ} is shown to increase with increasing speed up to the maximum test speed $M = 0.68$ when the elevator gap was sealed and the elevator with no appreciable fabric distortion (elevator 1) was tested.

The theoretical elevator effectiveness has been calculated according to the theory of reference 3 and is 20 percent higher than the experimental value obtained at $M = 0.20$. Since the thin-airfoil theory applies to flaps hinged at the leading edge and no correction is made for the increase in lift due to the balance area, the elevator with the balance area would be expected to have a higher effectiveness. Reasonable agreement is obtained, however, between the low-speed value of $\partial\alpha/\partial\delta$ of 0.51 for these tests and the experimental value of 0.55 of reference 4.

Pitching moment.- The variation of pitching-moment parameters with Mach number is shown in figure 9. The parameters C_{m_α} and C_{m_δ} (fig. 9) increase in absolute value with increasing Mach number. The parameter $\left(\partial C_m/\partial C_L\right)_\alpha$ gives the position of the aerodynamic center with respect to the quarter-chord point of the calculated mean aerodynamic chord. The variation of the parameter $\left(\partial C_m/\partial C_L\right)_\alpha$ with Mach number is presented in figure 9. When the lift is obtained by changing the angle of

attack, $\left(\partial C_m/\partial C_L\right)_\delta$ at $\delta = 0^\circ$, the aerodynamic center of the airfoil shifts forward from 0.227c at $M = 0.20$ to 0.160c at $M = 0.70$. When the lift is obtained by changing the elevator angle at $\alpha = 0^\circ$, the aerodynamic center of the airfoil shifts rearward from 0.520c at $M = 0.20$ to 0.670c at $M = 0.70$. However, these changes in the location of the aerodynamic center will have negligible effect on the stability and control of the airplane.

Hinge moment.- The effect of increasing Mach number on the elevator hinge-moment parameters is shown in figure 10. In general, the overbalance of C_{h_α} and the underbalance of C_{h_δ} increased with increasing Mach number. In the absence of boundary-layer changes, the elevator hinge-moment coefficient might logically be assumed to increase in absolute value with speed according to Glauert's factor $\left(1 - M^2\right)^{-1/2}$. However, the increase in C_{h_δ} with Mach number is approximately three times this factor at $M = 0.70$. Furthermore, the increase in C_{h_δ} represents an increase of approximately 100 percent in the hinge-moment coefficient. (See reference 2.) Also shown in figure 10 are the values for zero and 100 percent aerodynamic balance and balance effectiveness. The values for zero aerodynamic balance have been calculated according to the theory presented in references 5 and 6 and, as such, do not include compressibility effects. However, the low-speed values have been extended through the speed range tested to provide an approximate criterion for judging the experimental values.

Effect of Trailing-Edge Angle

The low-speed values of C_{h_α} and C_{h_δ} obtained with the metal elevator (trailing-edge angle 13°) were 0.0020 and -0.0015, respectively. The results of tests made at the Langley Laboratory of a scale model of the complete airplane and experience with flight investigations on other airplanes have shown that the value of C_{h_α} should be approximately zero in order to avoid adverse effects on the stability and control characteristics, particularly in gusty air. Preliminary calculations based on unpublished data indicated that zero C_{h_α} could be obtained by decreasing the trailing-edge angle from approximately 13° to 7°. This change in elevator shape was obtained by the use of solid wood elevators and is illustrated in figure 3.

Hinge moment.- The effect of trailing-edge angle on the elevator hinge-moment coefficient is shown in figure 11 for three angles of attack and $M = 0.35$. The nonlinearity of these curves prevents the exact use of the usual parameters, but the 6° change in elevator trailing-edge angle resulted in changes in the parameters of approximately $\Delta C_{h_\delta} = -0.0013$ and $\Delta C_{h_\alpha} = -0.0026$. The change in C_{h_α} due to reducing the trailing-edge angle was of the desired magnitude, but the accompanying increase in C_{h_δ} was undesirable. The undesirable increase in C_{h_δ} due to reducing the trailing-edge angle may be nullified with no appreciable change in C_{h_α} by changing the elevator nose shape. (See section entitled "Effect of Nose Shape.")

Effect on drag.- The variation of the drag coefficient for elevators 1 and 2 ($\phi = 13°$ and 7°, respectively) with elevator angle is presented in figure 12 for three angles of attack and $M = 0.35$. The increase in drag for a given increment of elevator deflection is slightly more for elevator 2 ($\phi = 7°$) than for elevator 1 ($\phi = 13°$).

Effect on lift.- In general, a decrease in elevator trailing-edge angle was accompanied by a slight increase in lift. Reducing the trailing-edge angle from 13° to 7° increased C_{L_α} from 0.061 to 0.064 and C_{L_δ} from 0.031 to 0.032.

Effect on pitching moment.- Reducing the trailing-edge angle from 13° to 7° caused the center of lift to be shifted rearward. The center of lift shifted from 22.6 to 24.2 percent of the mean aerodynamic chord for $\delta = 0°$ when the lift was varied by changing the angle of attack. The center of lift was shifted from 56 to 57.7 percent of the mean aerodynamic chord for $\alpha = 0°$ when the lift was varied by changing the elevator angle. These changes agree qualitatively with other investigations (reference 7).

Effect of Nose Shape

The results of these tests for trailing-edge configurations showed that the desired value of C_{h_α} could

be obtained with a trailing-edge angle of approximately 7°. The reduction in trailing-edge angle, however, caused an appreciable increase (-0.0013) in the value of C_{h_δ}. Since the original value of C_{h_δ} obtained for the metal elevator (-0.0015) was considered satisfactory by the manufacturer, it was desirable to reduce the new value of C_{h_δ}. Reference 8 shows that the value of C_{h_δ} can be changed, without appreciably affecting the value of C_{h_α}, by altering the elevator nose shape. Accordingly, systematic alterations were made to the nose profile until a satisfactory value of C_{h_δ} was obtained. (See fig. 3.)

Hinge moment.- The effect of the nose modifications on the hinge-moment coefficient at a Mach number of 0.35 is shown in figures 13 and 14. The nonlinearity of the variation of the hinge-moment coefficient with elevator angle prevents an exact measure of the parameter C_{h_δ}. Also, the difference in structural stiffness between the wooden and metal elevators and the asymmetry of the metal elevator prevents a direct comparison of the hinge-moment parameters of the two elevators. Therefore, elevator 4, which had a semielliptical nose profile like the metal elevator, is used as a reference and only the incremental changes in C_{h_δ} and C_{h_α} due to nose modifications are presented. Figures 13 and 14 indicate that modifying the elevator nose profile to modified blunt shape (elevator 3) results in $\Delta C_{h_\delta} = 0.0010$ and $\Delta C_{h_\alpha} = 0.0002$, approximately, and modifying the elevator nose to the blunt shape (elevator 2) results in $\Delta C_{h_\delta} = 0.0020$ and $\Delta C_{h_\alpha} = 0.0004$; consequently, an elevator that has a slightly greater balance-moment area than elevator 3 will provide the desired decrease in C_{h_δ} of 0.0013 and so nullify the adverse effect of reducing the trailing-edge angle to 7°. The tests of the wooden elevator therefore indicate that the desired values of $C_{h_\alpha} \approx 0$ and $C_{h_\delta} = -0.0015$ at $M = 0.35$ may be obtained if the original metal elevator profile is modified so that it has a modified blunt nose shape (elevator 3) and a cusped contour behind the hinge line (elevator 2).

The incremental changes in C_{h_δ} due to the elevator nose-contour modifications are of the same order of magnitude as would be calculated by the method of

reference 8. As might be expected, very poor agreement is obtained when the value of C_{h_δ} for any one elevator is calculated from the unbalanced section flap data and corrected for balance effects by this method. More precise methods for correcting section hinge-moment data to finite aspect ratio are being developed at the present time.

Lift.- The effect of elevator nose contour on C_{L_δ} is shown in figure 15 at $\delta = 0°$, $M = 0.35$, and $\alpha = -3°$ to $3°$. Figure 15 shows that the lift increases slightly as the surface discontinuity between the rear portion of the stabilizer and the elevator nose is reduced because, as the contour of the tail surface approaches that of the true airfoil, optimum pressure distribution and lift are obtained.

Drag.- The effect of elevator nose contour on drag is also shown in figure 15. The drag increases slightly as the surface discontinuity between the rear portion of the stabilizer and the elevator nose is increased.

Pitching moment.- The effect of elevator nose contour on the pitching moment was not appreciable and no data are presented.

Effect of Trailing-Edge Strips

Temporary changes in elevator characteristics are often made by the use of trailing-edge strips. An investigation was therefore undertaken to determine, for this full-scale tail surface, the combinations of length and diameter of trailing-edge strips that could be used on the original elevator as a temporary expedient to obtain $C_{h_\alpha} = 0$. Various lengths of $\frac{1}{8}$-inch- and $\frac{1}{16}$-inch-diameter strips were tested at $M = 0.35$ and $\alpha = -3°$, $0°$, and $3°$.

Hinge moment.- Figures 16 and 17 show the variation of hinge-moment coefficient with elevator angle for various lengths of $\frac{1}{8}$-inch- and $\frac{1}{16}$-inch-diameter trailing-edge strips, respectively, at $\alpha = -3°$, $0°$, $3°$, and $M = 0.35$. Decreasing the length of the strip decreases the slope of the hinge-moment curves, and no abrupt changes in the trend of the curves occur. The data

presented in these figures have been used to obtain the hinge-moment parameters C_{h_α} and C_{h_δ} shown in figure 18. The desired value of $C_{h_\alpha} = 0$ can be obtained by use of a $\frac{1}{8}$-inch-diameter trailing-edge strip extending across 24 percent of the span or a $\frac{1}{16}$-inch-diameter strip extending across 38 percent of the span and centrally located on the elevator, at the expense, however, of an undesirable increase in C_{h_δ}. The effect of speed on the effectiveness of the trailing-edge strips is shown in figure 19. No serious change of hinge-moment coefficient or C_{h_α} occurs up to $M = 0.65$ with the full-span $\frac{1}{8}$-inch-diameter strips on the elevator trailing edge.

Of interest is the fact that the effects of the trailing-edge strips on the hinge-moment-coefficient parameters, C_{h_α} and C_{h_δ}, and the lift parameter C_{L_δ} are directly opposite to the effects due to beveling the trailing edge; that is, the use of trailing-edge strips results in increases in the values of C_{h_α}, C_{h_δ}, and C_{L_δ}, whereas beveling a trailing edge causes decreases in the values of these parameters.

Lift.- The effect of varying the length of the trailing-edge strips on lift coefficient is shown in figure 20 for the $\frac{1}{8}$-inch-diameter strip and in figure 21 for the $\frac{1}{16}$-inch-diameter strip. The use of full-span strips of either diameter results in an appreciable increase in lift at the high elevator angles. This increase in lift, however, affects only the value of C_{L_δ}, the value of C_{L_α} remaining practically constant. The value of C_{L_δ} increases linearly with strip length; the increase for the $\frac{1}{8}$-inch- and $\frac{1}{16}$-inch-diameter strips is 17 and 15 percent, respectively, when the strip length is increased from zero-span length to full-span length.

Drag.- The effect of the length of the trailing-edge strips on drag coefficient for $\frac{1}{8}$-inch- and $\frac{1}{16}$-inch-diameter strips is shown in figures 22 and 23, respectively. In general, the increase in drag due to

lengthening the strips for the $\frac{1}{8}$-inch-diameter strips is double the increase which occurred with the $\frac{1}{16}$-inch-diameter strips. The maximum increase in drag coefficient measured with $\frac{1}{8}$-inch-diameter, full-span strips was 13 percent.

Pitching moment.- The center of lift was shifted from 23 percent to 25 percent of the mean aerodynamic chord for $\delta = 0^\circ$ when the lift was increased by changing the angle of attack. The maximum shift in the aerodynamic center was from 52 percent to 58 percent of the mean aerodynamic chord for $\alpha = 0^\circ$ when the lift was increased by changing the elevator angle.

Effect of Lowering the Elevator with Respect to the Stabilizer

The data presented in the section entitled "Basic Data with Metal Elevator" indicated that the metal elevator trimmed at approximately -5° for $\alpha = 0^\circ$, which is believed to be a result of an error in the hinge location (see "Description of Model") and possibly some asymmetry in the elevator contour. A limited number of tests were therefore made with the metal elevator lowered to be more nearly alined with the stabilizer in order to determine the effect of this change.

Hinge moment.- The effect of lowering the hinge line on the elevator hinge moment is shown in figure 24 for three angles of attack and $M = 0.35$. The new hinge position results principally in a shift of the hinge-moment-coefficient curves for a limited range of elevator angles. The elevator trim angle at $\alpha = 0^\circ$ is changed from -5° to -1°.

Effect on lift, drag, and pitching moment.- No data are presented to show the effect of lowering the hinge line on C_L, C_D, and C_m because the effect was negligible.

Transition Strips

An investigation to determine the extent of laminar flow on the stabilizer was undertaken. Carborundum strips which are described in detail under "Methods and Apparatus" were used to fix the transition location.

Effect on drag.- Fixing the transition ahead of its normal location should result in an appreciable increase in drag. No pronounced increase in drag occurred as the transition strip was moved forward on the upper surface (fig. 25) to the 0.05c location, and it is therefore concluded that only a limited region of laminar flow existed, possibly 0.10c. The lack of laminar flow cannot be attributed to tunnel air-stream turbulence, since the turbulence factor for this tunnel is of the same order of magnitude as the factor for the low-turbulence tunnel, and extensive laminar flow is usually obtained on smooth models. Surface irregularities near the stabilizer nose, particularly a spanwise joint at 0.10c, are probably responsible for fixing the transition location. Figure 26 shows the effect on drag of locating the transition strips on the upper and lower surface of the stabilizer at 5 percent chord at $\delta = 0^\circ$ for $M = 0.20$, 0.45, and 0.60. The increment of drag caused by the transition strips remains almost constant for $\alpha = -3^\circ$ to 3° and $M = 0.20$ to 0.60 and essentially equal to the increase shown in figure 25.

Effect on elevator hinge moment.- The effect on elevator hinge moment of moving the transition strip forward is shown in figure 25 for $\delta = 0^\circ$ and 4°, $\alpha = 0^\circ$, and $M = 0.45$. The hinge moment decreases slightly as the transition strip is moved forward. This effect is believed to be due to thickening of the boundary layer.

Effect on lift and pitching moment.- The effect of the transition-strip location on C_L and C_m was not appreciable for any of the conditions tested.

Aerodynamic Hysteresis

Attempts to check some of the hinge-moment data revealed apparent discrepancies, the magnitude of which appreciably exceeded the accuracy of the measurements. An investigation to determine the source of these discrepancies revealed that, for a given model configuration,

two values of hinge moment could be obtained, depending on the direction from which the desired elevator angle was approached.

Effect on hinge moment.- Figure 27 shows the aerodynamic hysteresis effect for elevator 1. In general, the hysteresis was present for about 15° of the elevator travel. The maximum deviation due to hysteresis is approximately 2° of elevator angle. The hysteresis effect shown in figure 27 is representative of all of the elevators tested which had a straight contour behind the hinge line. Cusping the elevator contour behind the hinge line and so reducing the trailing-edge angle to 7° resulted in the virtual disappearance of the aerodynamic hysteresis. Also the hysteresis disappeared for all practical purposes at Mach numbers greater than about 0.65. The aerodynamic hysteresis is probably related to local boundary-layer separation on the rear part of the elevator. It is an obviously undesirable phenomenon, which would possibly necessitate continuous small adjustments of the airplane trimming mechanism in flight.

Effect on lift, drag, and pitching moment.- Inasmuch as the hysteresis was related to the elevator contour behind the hinge line, only a fraction of the total area was affected. As would be expected, the effect on lift, drag, and pitching moment was found to be negligible and no data are presented.

Elevator Pressure

The metal skin on both the upper and lower surfaces of the elevator at station 50 (fig. 28) bulged and failed by tearing out from under the rivet heads at approximately $0.75c_e$ as a result of either a large local pressure difference across the elevator skin or local stress concentrations. (See fig. 29.) The external and internal pressures of the elevator were therefore measured to determine whether a local aerodynamic condition was causing the failure.

Two pressure belts were used to measure the external pressures on the upper surface. One belt was located at station 47 and a small belt at the station of failure (station 50). No appreciable differences were noted, however, in the external pressures at stations 47 and 50, and only the pressures at station 47 are shown in

figure 30. This figure shows no irregular or excessive external pressures in the area of failure ($0.75c_e$) at $M = 0.20$. Additional tests made at $M = 0.35$ and 0.45 showed similar results and the bulge was therefore concluded to be a result of a local structural weakness.

The possibility of venting the elevator in order to nullify the pressure drop across the skin and thus to eliminate the skin deflection was investigated. It was necessary to determine the internal pressure of the elevator before attempting to choose a vent location. Figure 31 presents the effect of elevator angle on the internal pressure coefficient P_i at $\alpha = 0^\circ$ and $M = 0.20$. The internal pressure was measured with normal leakage into the elevator and with all apparent openings such as the elevator hinge pockets sealed. A comparison of figures 30 and 31 shows that the normal elevator leakage provides probably the highest negative internal pressure and therefore the lowest pressure difference across the elevator skin; thus air vents would be of no practical benefit. It must be concluded that structural loads cause local stress concentrations at the middle hinge pocket and result in failure of the skin at this location.

CONCLUSIONS

The following conclusions may be drawn from the investigation described in this report:

1. A large increase in hinge-moment parameter C_{h_δ} (rate of change of hinge-moment coefficient with elevator deflection) occurred for the metal elevator as the Mach number M was increased. The low-speed value of -0.0015 at $M = 0.20$ increased to -0.0032 at $M = 0.70$. The hinge-moment parameter C_{h_α} (rate of change of hinge-moment coefficient with angle of attack) changed from 0.0024 at $M = 0.20$ to 0.0027 at $M = 0.70$ with a minimum value of 0.0020 at $M = 0.35$.

2. The metal elevator effectiveness decreased with increasing speed. This effect is believed to be a result of the elevator gap being unsealed. The low-speed value of 0.51 at $M = 0.020$ decreased to 0.34 at $M = 0.70$.

3. The values of $C_{h_\delta} = -0.0015$ and $C_{h_\alpha} \approx 0$ desired for this tail surface when used on the airplane for which it was designed may be obtained by modifying the original elevator to have a modified blunt nose (elevator 3) and a cusped contour behind the hinge line (elevator 2).

4. The incremental changes in C_{h_δ} due to elevator nose-shape modifications were of about the same magnitude as would be predicted by the use of recently published methods.

5. Trailing-edge strips of $\frac{1}{8}$-inch diameter and 24 percent span length on the metal elevator reduced the value of $C_{h_\alpha} = 0.0020$ to zero, but with an accompanying increase in C_{h_δ} from -0.0015 to -0.0040 at $M = 0.35$. No appreciable loss of trailing-edge-strip effectiveness in changing C_{h_α} was apparent up to $M = 0.65$.

6. The region of laminar flow over the stabilizer was limited to approximately 10 percent of the stabilizer chord.

Langley Memorial Aeronautical Laboratory
National Advisory Committee for Aeronautics
Langley Field, Va., March 11, 1946

REFERENCES

1. Swanson, Robert S., and Toll, Thomas A.: Jet-Boundary Corrections for Reflection-Plane Models in Rectangular Wind Tunnels. NACA ARR No. 3E22, 1943.

2. Schueller, Carl F., and Korycinski, Peter F.: Effect of Fabric Deflection at High Speeds on the Aerodynamic Characteristics of the Horizontal Tail Surface of an SB2D-1 Airplane. NACA ARR No. L5F10a, 1945.

3. Glauert, H.: Theoretical Relationships for an Aerofoil with Hinged Flap. R. & M. No. 1095, British A.R.C., 1927.

4. Sears, Richard I.: Wind-Tunnel Data on the Aerodynamic Characteristics of Airplane Control Surfaces. NACA ACR No. 3L08, 1943.

5. Perring, W. G. A.: The Theoretical Relationships for an Aerofoil with a Multiply Hinged Flap System. R. & M. No. 1171, British A.R.C., 1928.

6. Goett, Harry J., and Reeder, J. P.: Effects of Elevator Nose Shape, Gap, Balance, and Tabs on the Aerodynamic Characteristics of a Horizontal Tail Surface. NACA Rep. No. 675, 1939.

7. Purser, Paul E., and Riebe, John M.: Wind-Tunnel Investigation of Control-Surface Characteristics. XV - Various Contour Modifications of a 0.30-Airfoil-Chord Plain Flap on an NACA 66(215)-014 Airfoil. NACA ACR No. 3L20, 1943.

8. Purser, Paul E., and Toll, Thomas A.: Analysis of Available Data on Control Surfaces Having Plain-Overhang and Frise Balances. NACA ACR No. L4E13, 1944.

TABLE I

PHYSICAL CHARACTERISTICS OF THE HORIZONTAL TAIL SURFACE

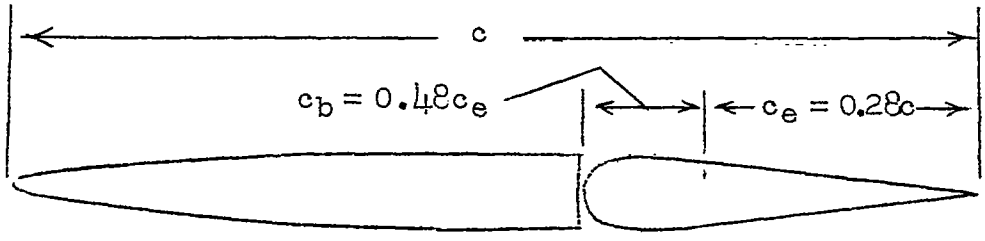

NACA 66-009 . $\lambda = .06905$

Airfoil section	Modified NACA 66-009
Semispan, b/2, in.	112.0
Root chord, c_r, in.	66.0
Tip chord, c_t, in.	33.0
Area of semispan, $S_w/2$, sq in.	5275.0
Mean aerodynamic chord, in.	51.3
Aspect ratio, A	4.76
Taper ratio	0.50
Area of stabilizer, S_s, sq in.	3259.0
Area of elevator, S_e, sq in.	1429.0
Area of overhang, S_b, sq in.	596.0
Root-mean-square elevator chord behind hinge line, $\overline{c}_e$, in.	13.74
Elevator overhang, c_b/c_e	0.48

NATIONAL ADVISORY
COMMITTEE FOR AERONAUTICS

TABLE II

COORDINATES FOR WOODEN ELEVATORS IN PERCENT CHORD

x	Elevator 1	Elevator 2	Elevator 3	Elevator 4
	y	y	y	y
0	0	0	0	0
.51	3.91	3.91	3.19	2.47
1.03	5.04	5.04	4.19	3.33
2.06	6.26	6.26	5.33	4.40
3.09	7.10	7.10	6.19	5.27
4.12	7.61	7.61	6.71	5.80
5.14	8.03	8.03	7.20	6.38
6.17	8.23	8.23	7.47	6.71
7.20	8.46	8.46	7.75	7.04
8.23	8.62	8.62	7.95	7.28
9.26	8.75	8.75	8.16	7.57
10.29	8.85	8.85	8.31	7.78
11.32	8.91	8.91	8.43	7.94
12.35	8.93	8.93	8.50	8.07
13.37	8.95	8.95	8.59	8.23
14.40	8.99	8.99	8.63	8.27
16.46	8.95	8.95	8.69	8.44
18.52	8.87	8.87	8.65	8.44
20.58	8.76	8.76	8.60	8.44
22.63	8.64	8.64	8.54	8.44
24.69	8.44	8.44	8.38	8.31
28.81	8.03	8.03	8.01	7.99
32.92	7.57	7.57	7.55	7.53
37.04	(a)	7.10	7.10	7.10
41.15		6.59	6.59	6.59
45.27		6.13	6.13	6.13
49.38		5.58	5.58	5.58
53.50		5.04	5.04	5.04
57.61		4.53	4.53	4.53
61.73		3.93	3.93	3.93
65.84		3.48	3.48	3.48
69.96		3.01	3.01	3.01
74.08		2.47	2.47	2.47
78.19		2.02	2.02	2.02
82.31		1.56	1.56	1.56
86.42		1.13	1.13	1.13
90.54		.82	.82	.82
94.65		.52	.52	.52
98.77		.27	.27	.27
Trailing-edge radius = 0.05 inch				

(a) Straight taper behind 32.4 percent chord.

NATIONAL ADVISORY
COMMITTEE FOR AERONAUTICS

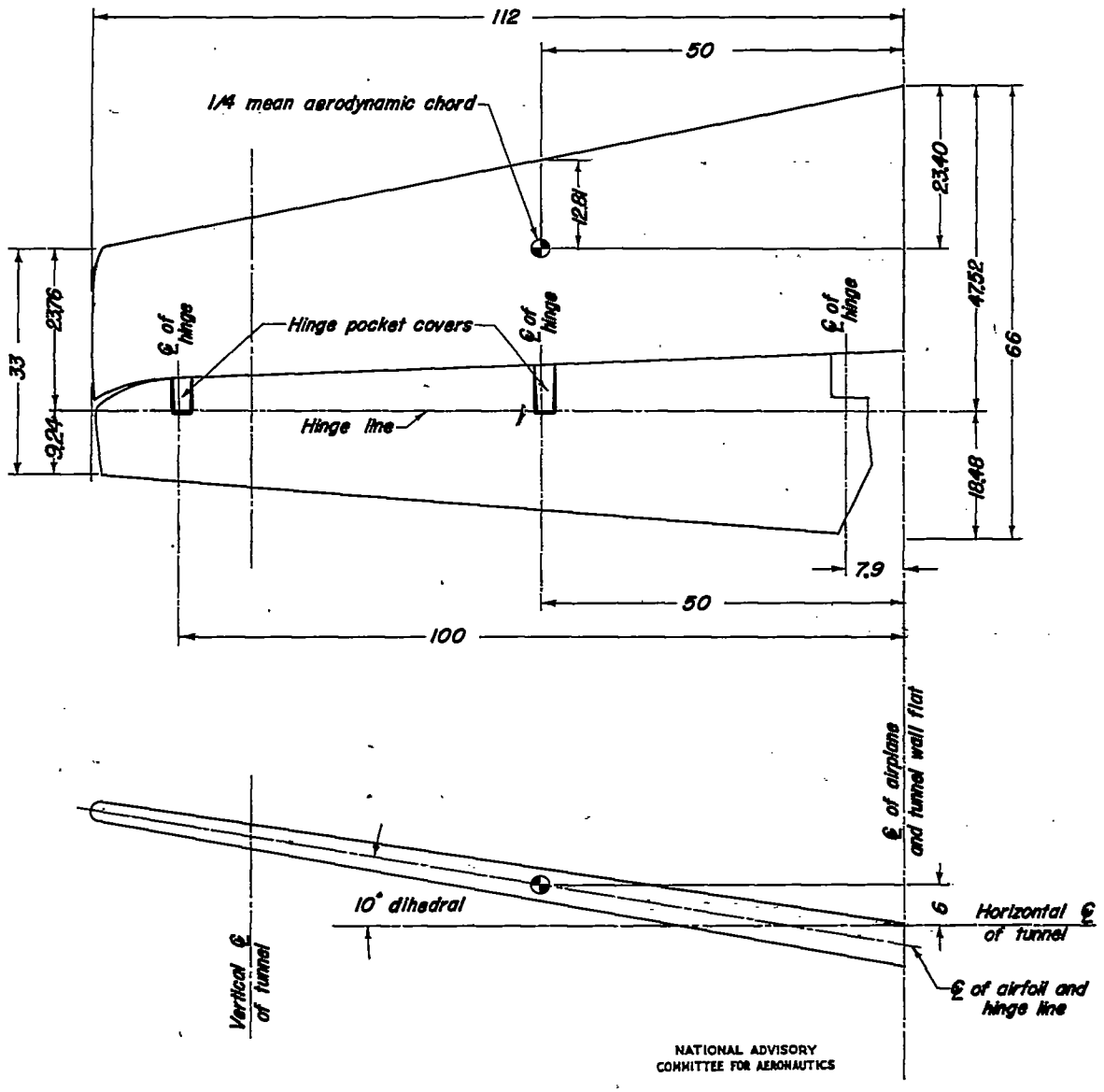

Figure 1.- General arrangement of the horizontal tail surface in the Langley 16-foot high-speed tunnel. All dimensions shown are in inches and are measured in the plane of the section.

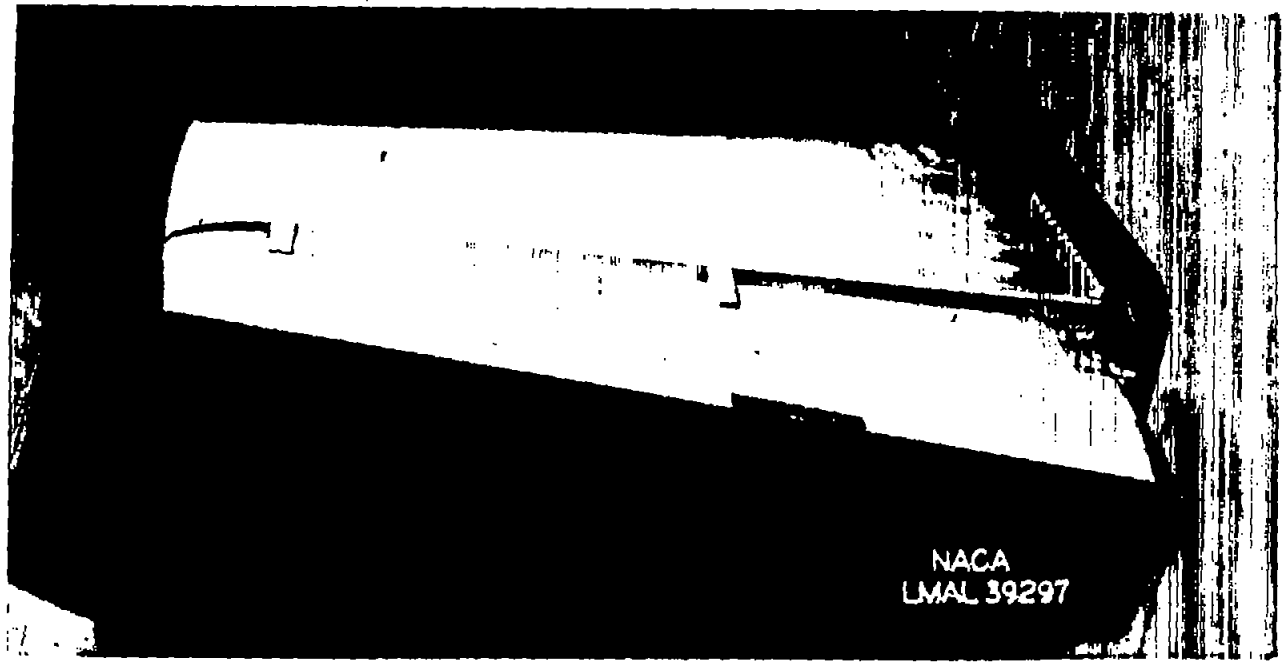

Figure 2.- General view of the semispan horizontal tail installed in the Langley 16-foot high-speed tunnel.

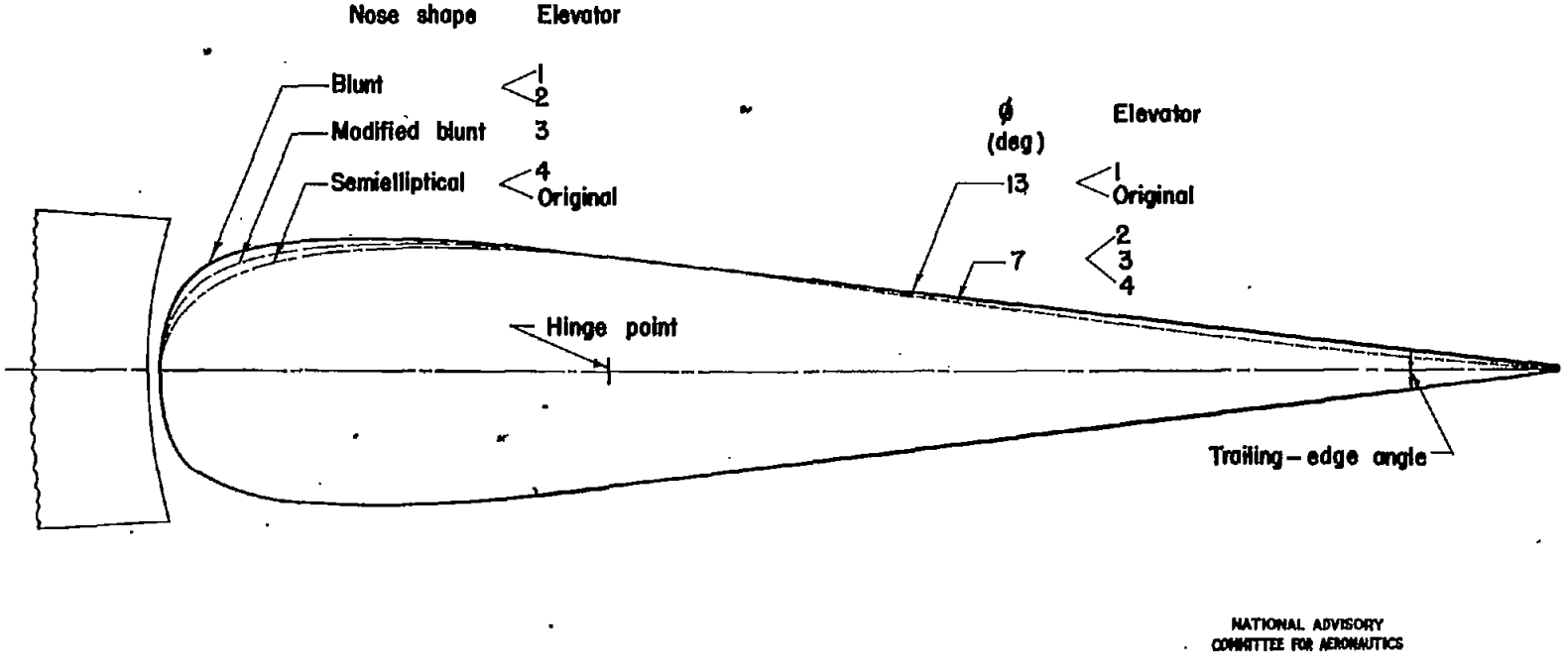

Figure 3.—Contours of original metal elevator and elevators 1 to 4.

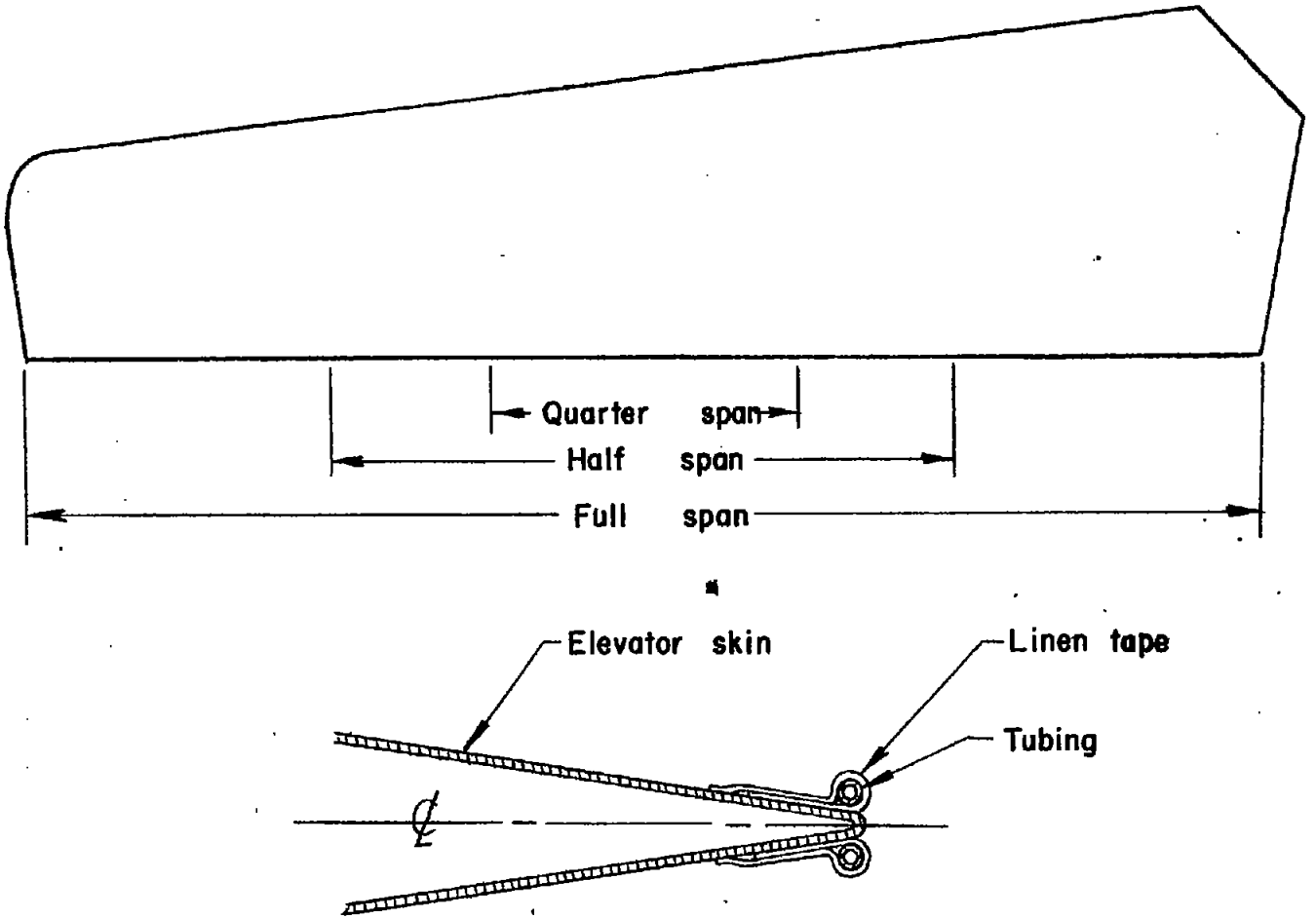

Figure 4.—Location and installation of trailing-edge strips on metal elevator.

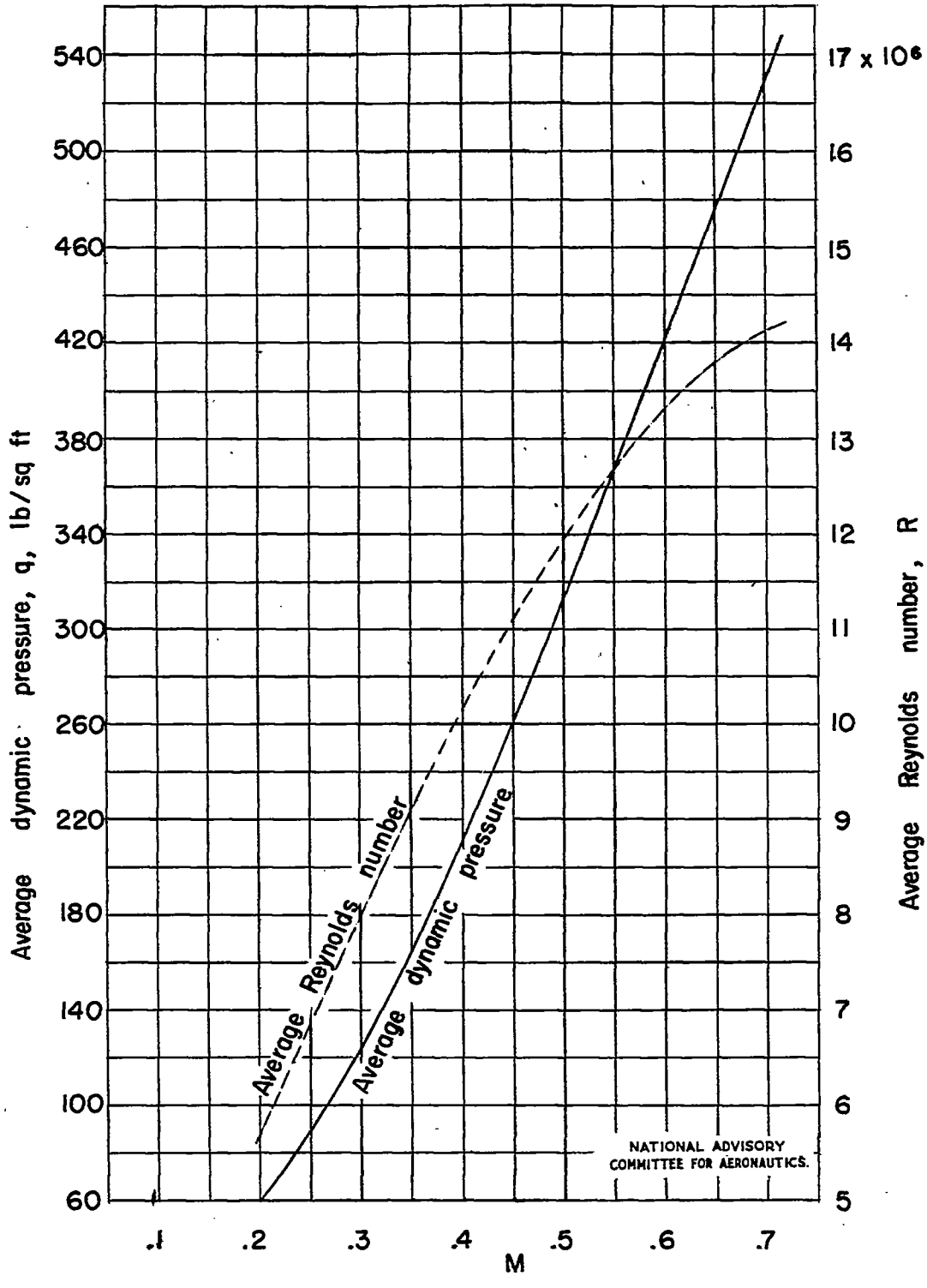

Figure 5. — Variation of the average dynamic pressure and average Reynolds number with test Mach number.

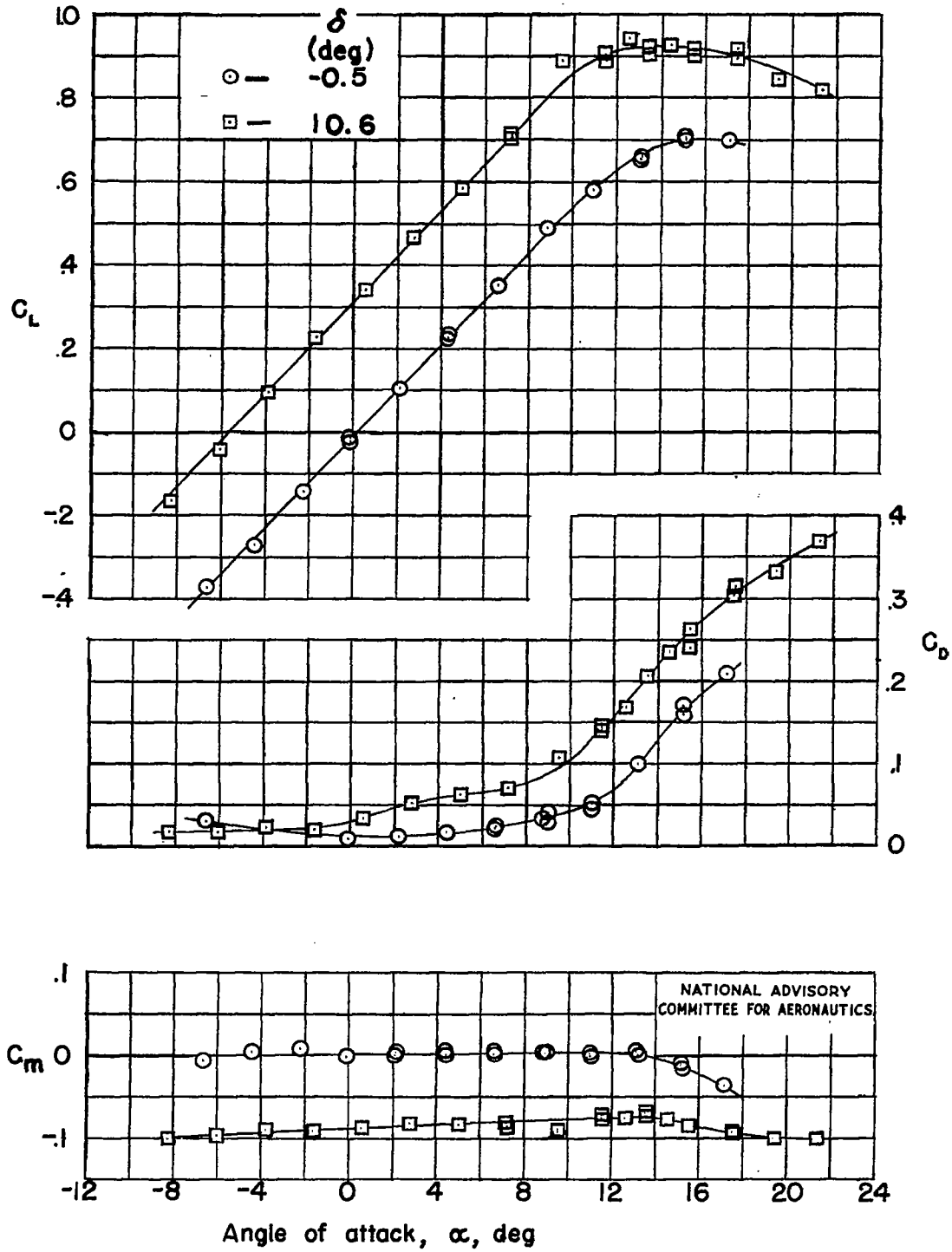

Figure 6.— Basic aerodynamic characteristics for two elevator angles. $\delta = -.5°$ and $10.6°$; M=0.20.

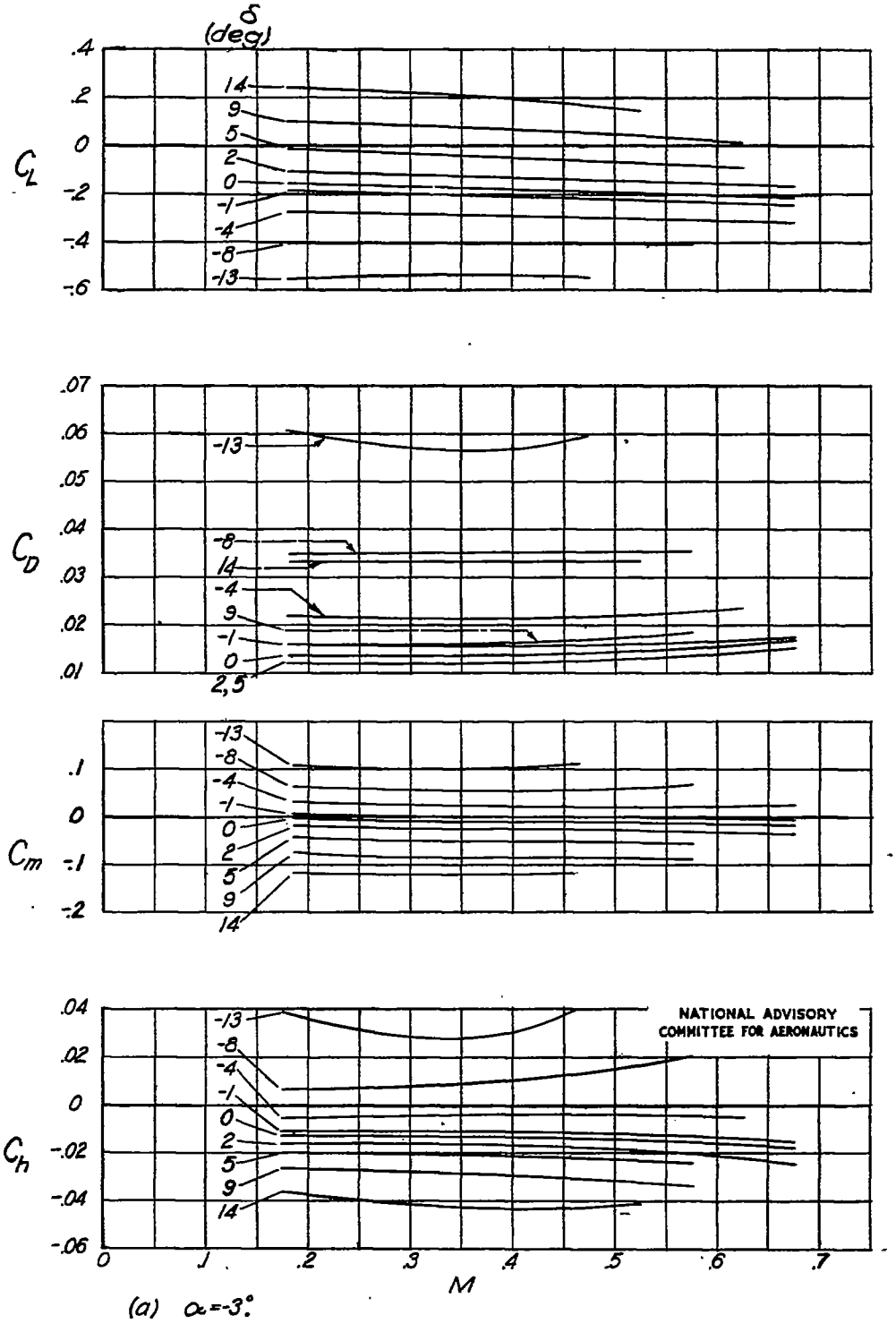

(a) $\alpha = -3°$.

Figure 7.– Variation of aerodynamic characteristics with Mach number. Metal elevator.

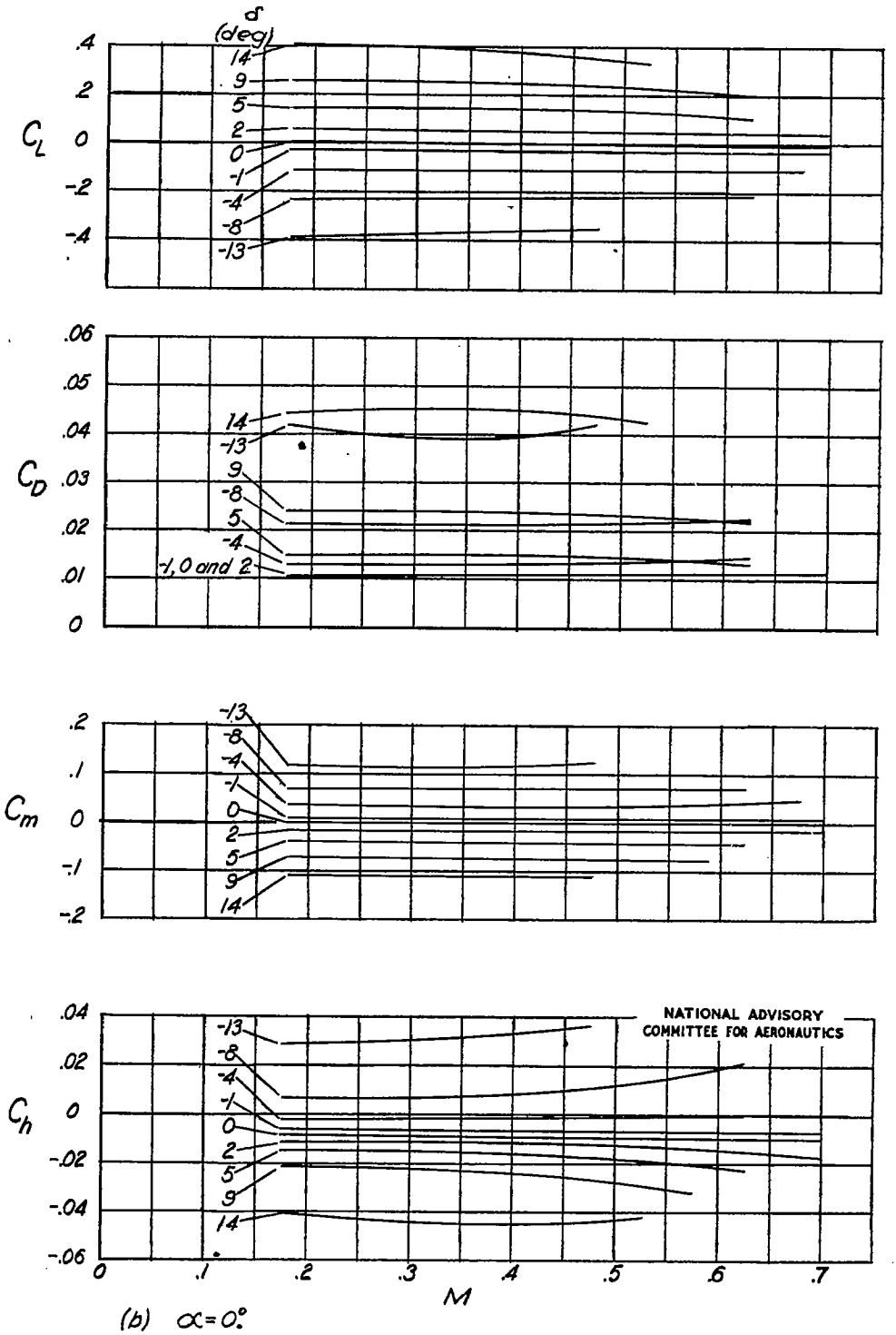

(b) $\alpha = 0°$

Figure 7.- Continued.

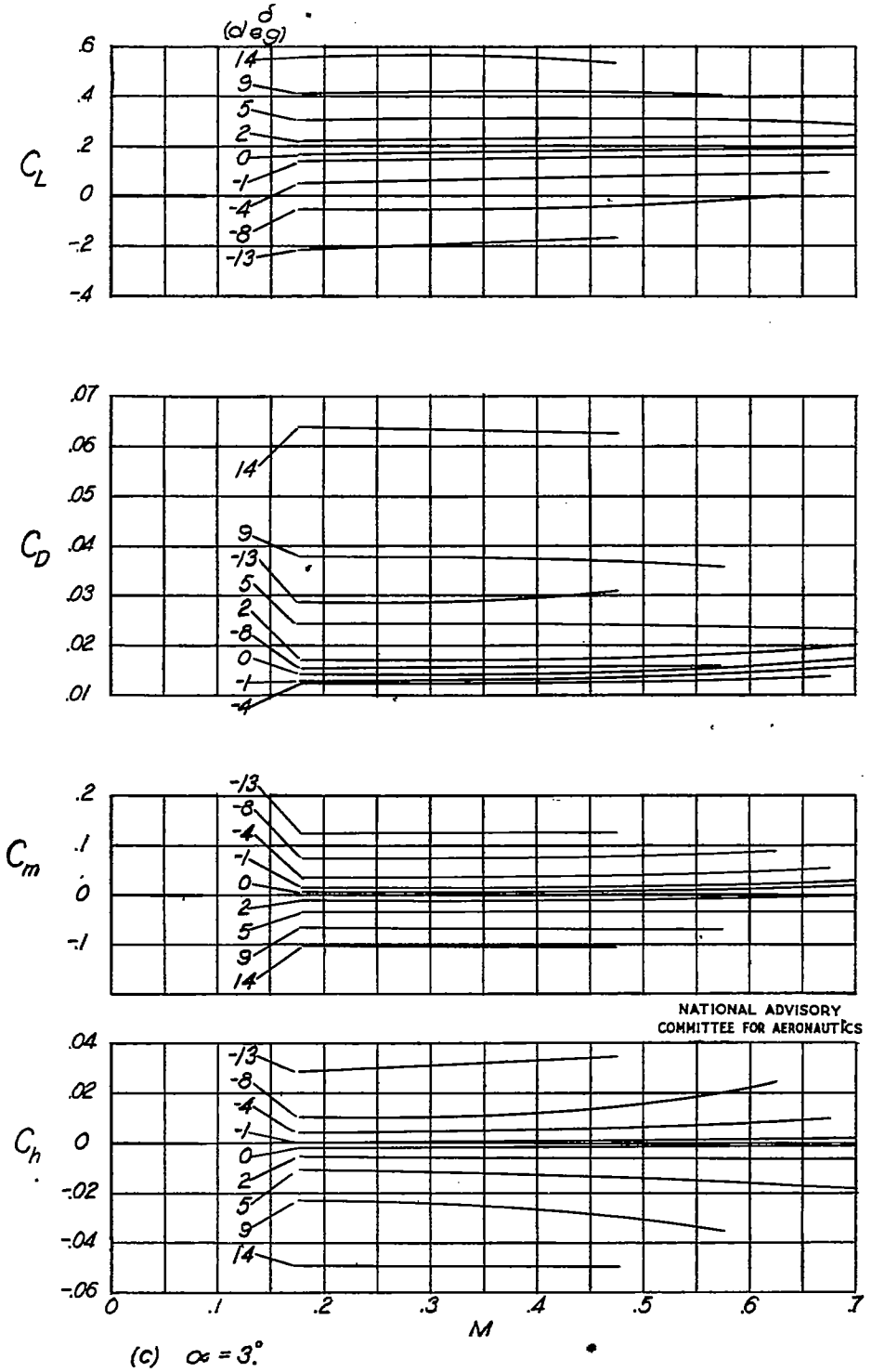

(c) $\alpha = 3°$

Figure 7.- Continued.

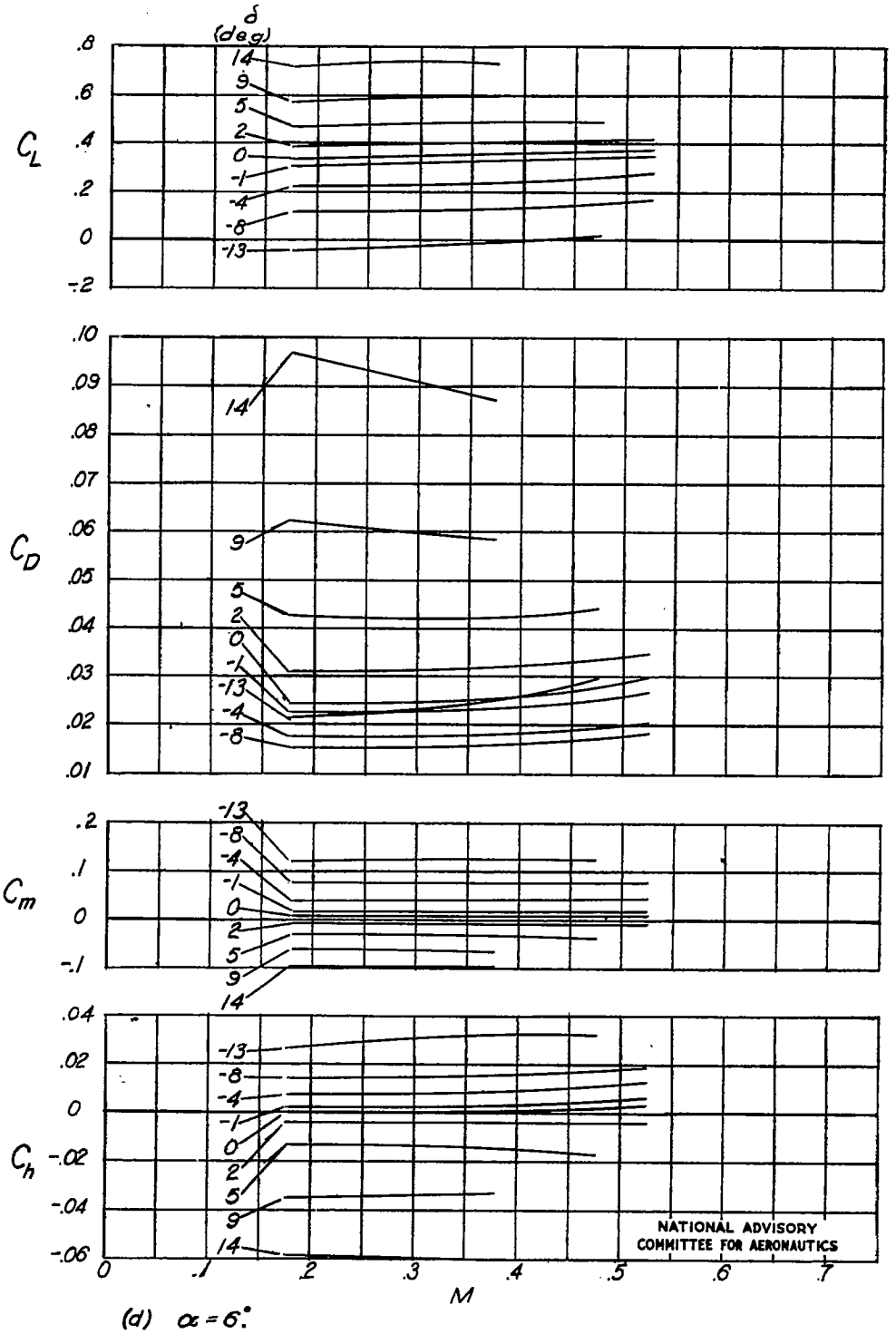

(d) $\alpha = 6°$

Figure 7.-Continued.

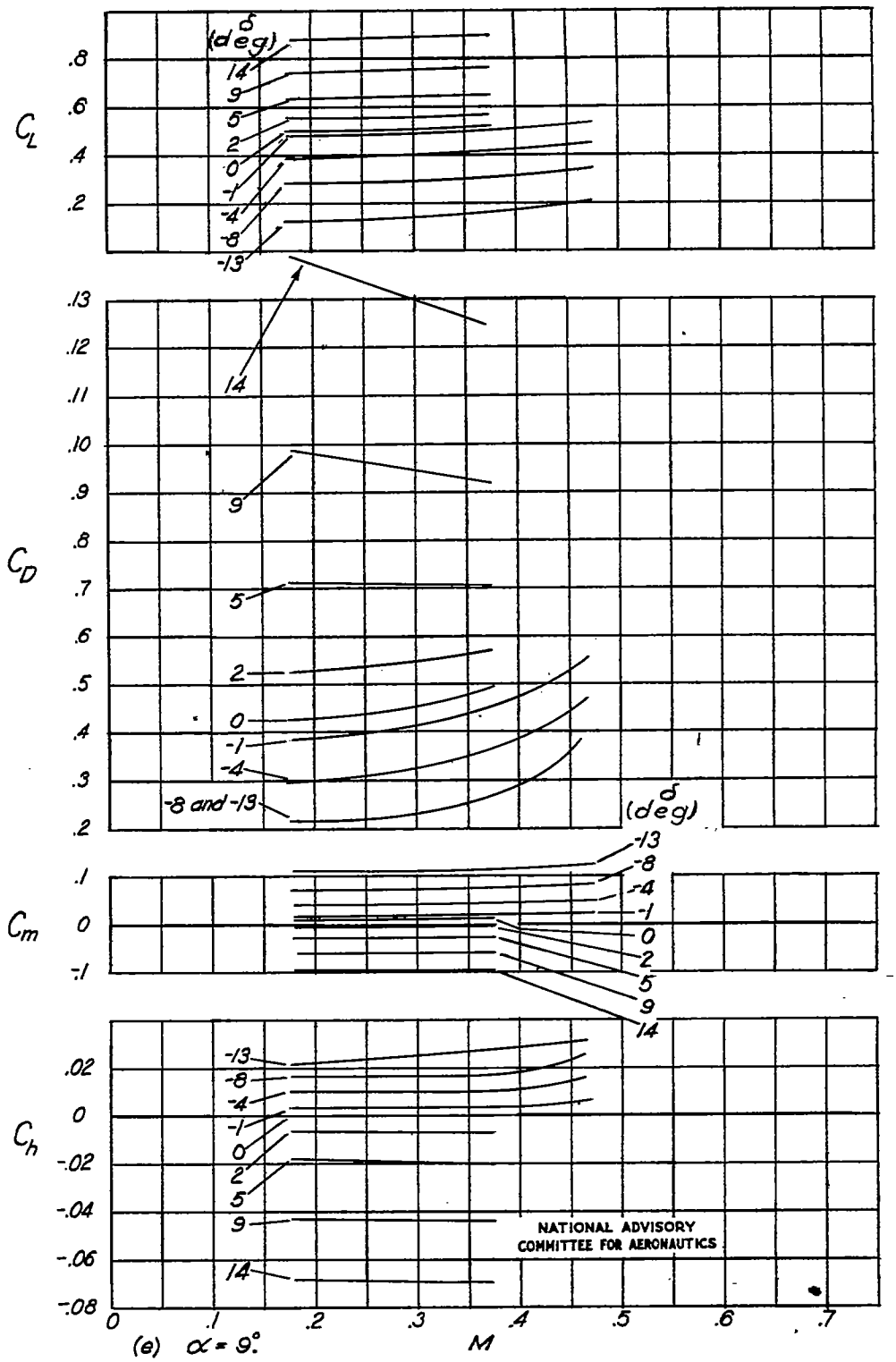

Figure 7.- Concluded.

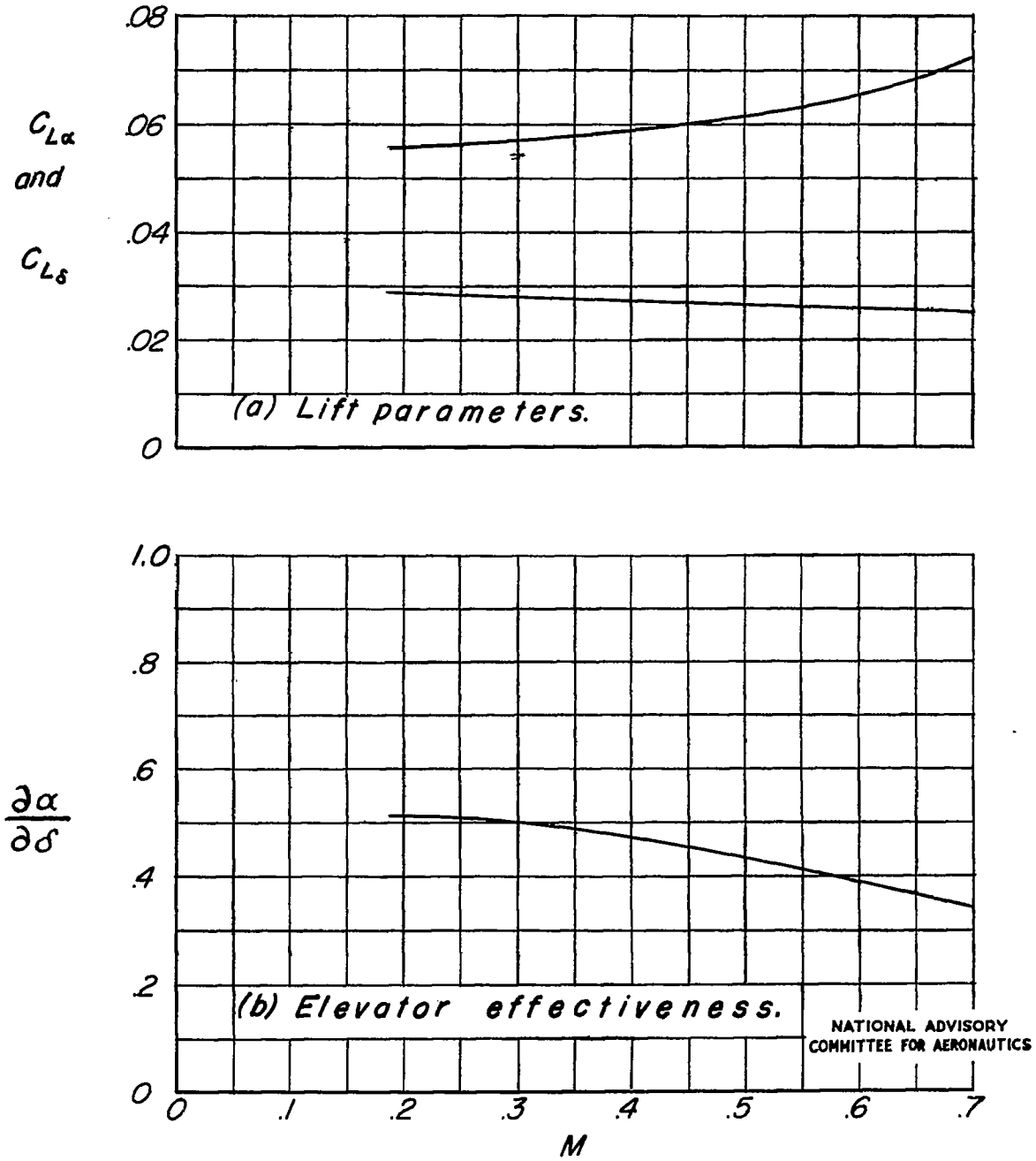

Figure 8.– Effect of Mach number on lift parameters and elevator effectiveness.

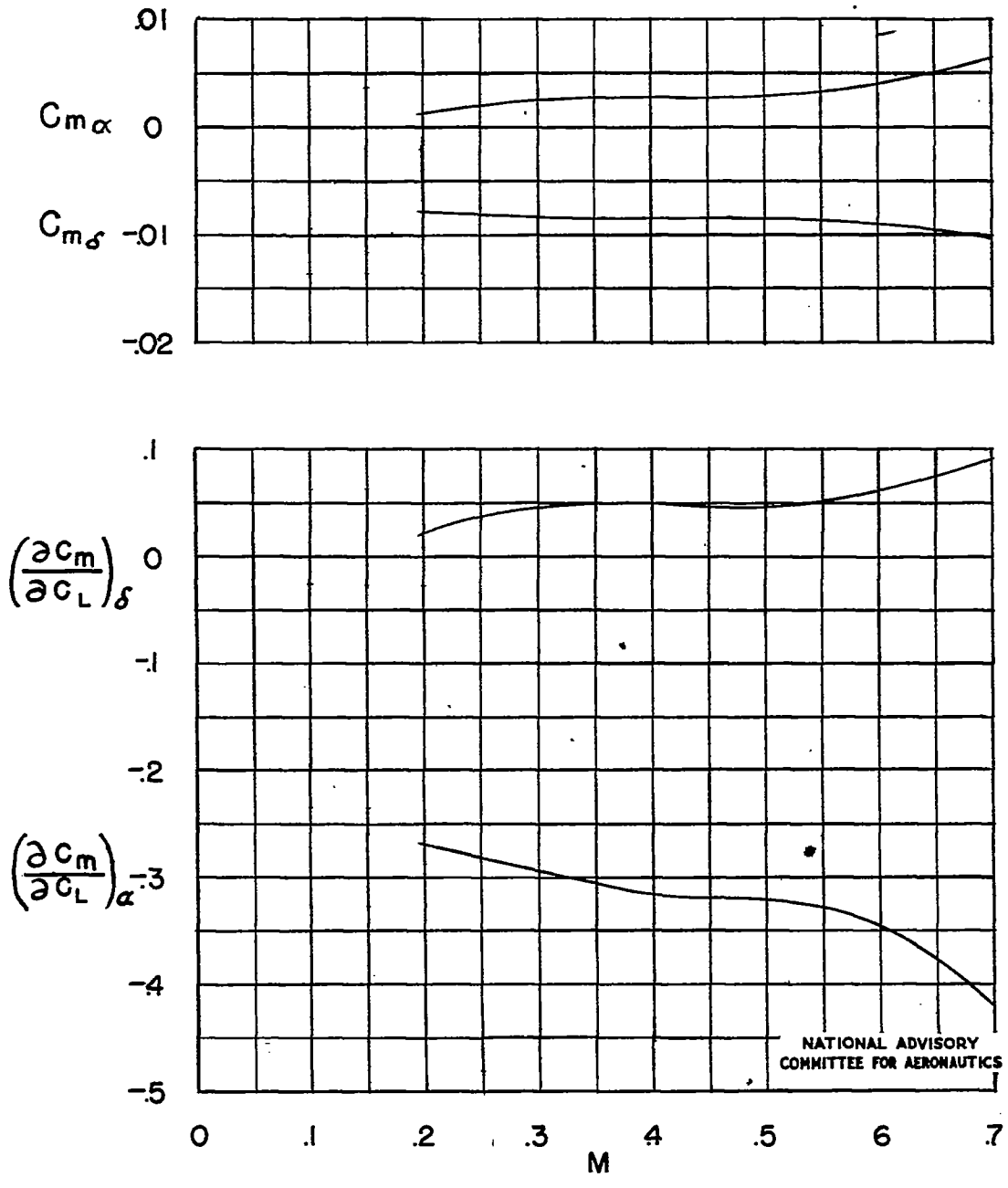

Figure 9 .—Variation of the pitching-moment-coefficient parameters with Mach number. Metal elevator.

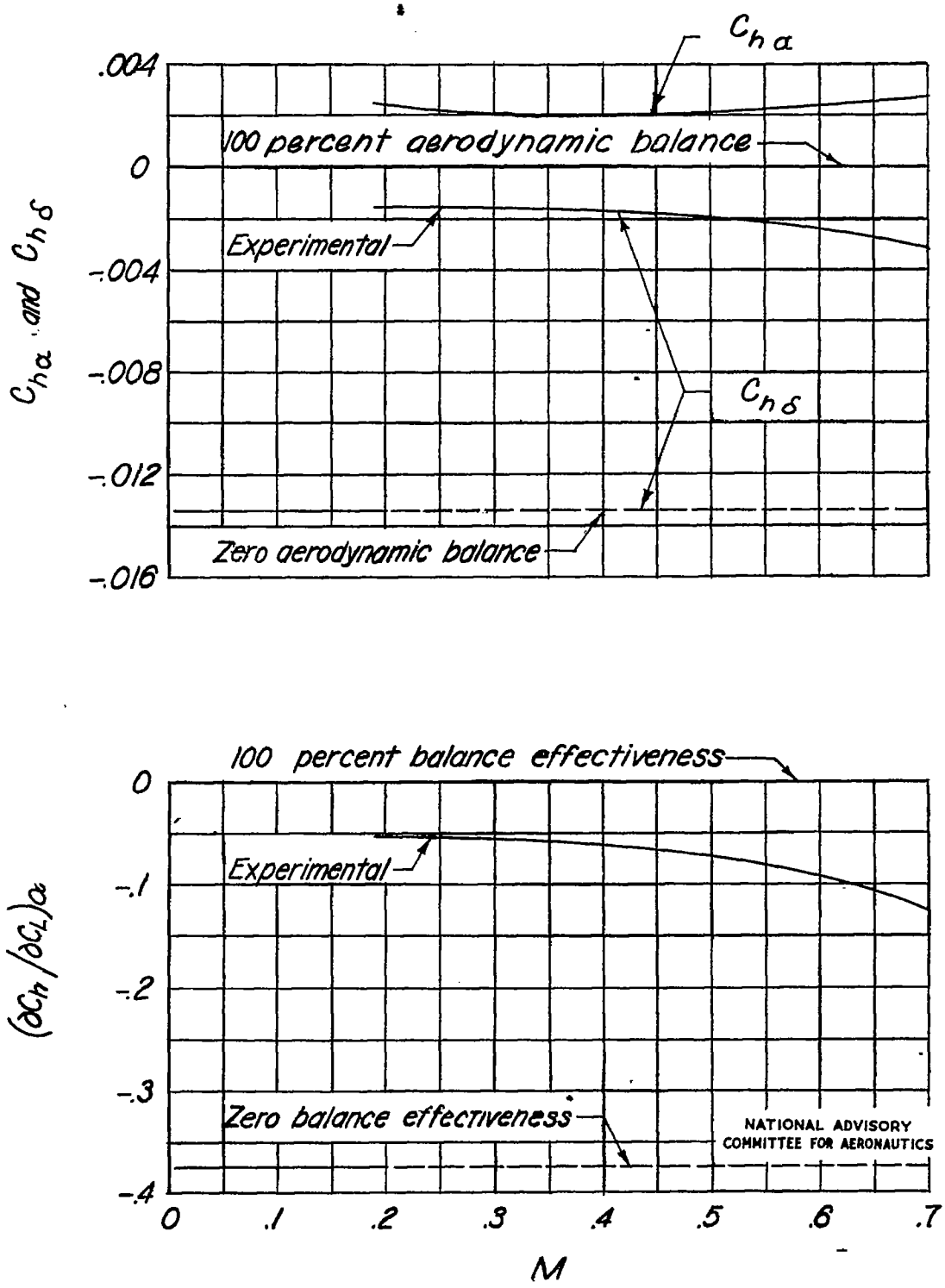

Figure 10.- The variation of the hinge-moment parameters with Mach number. Metal elevator.

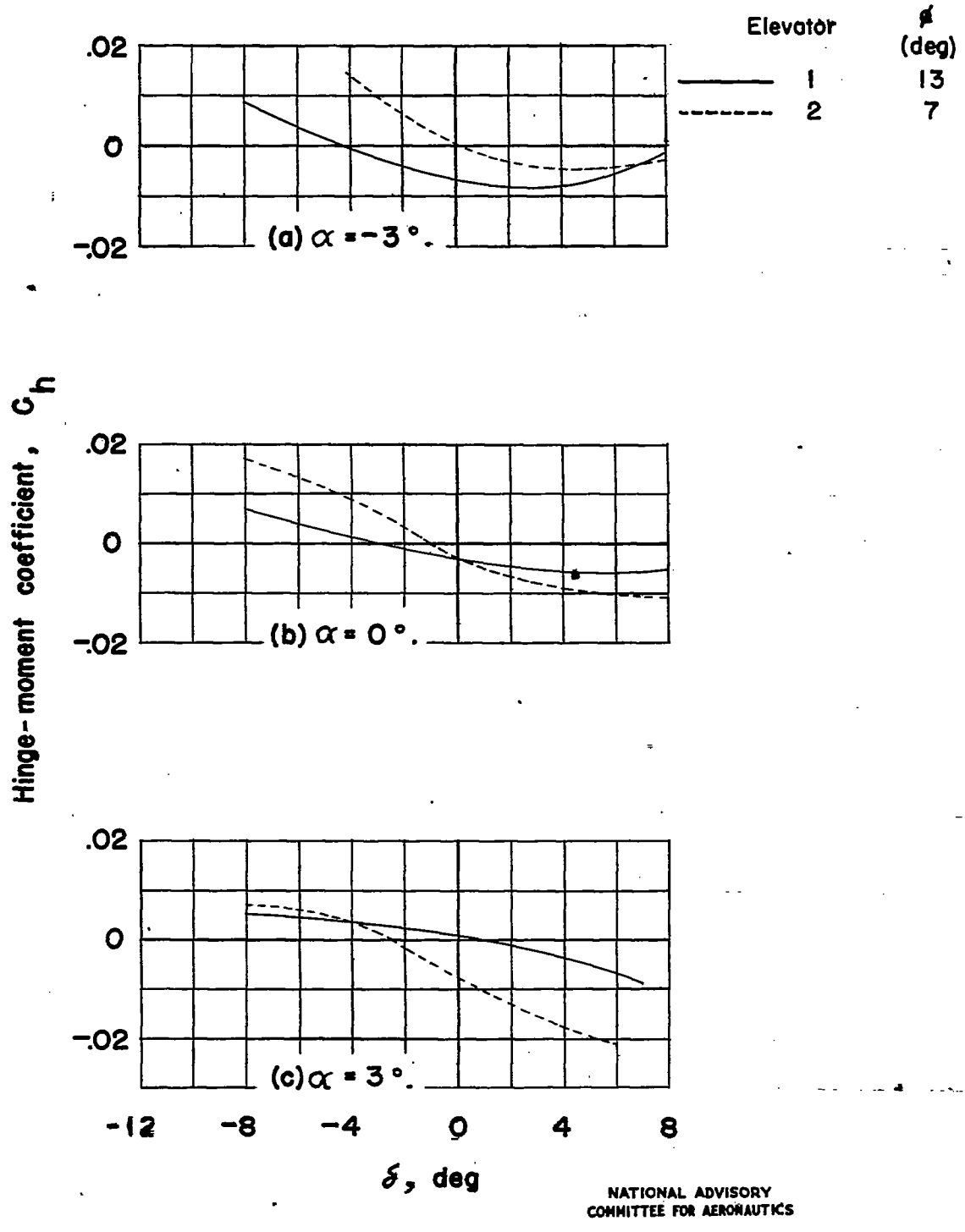

Figure 11. —Effect of elevator trailing-edge angle on elevator hinge-moment coefficient. M= 0.35.

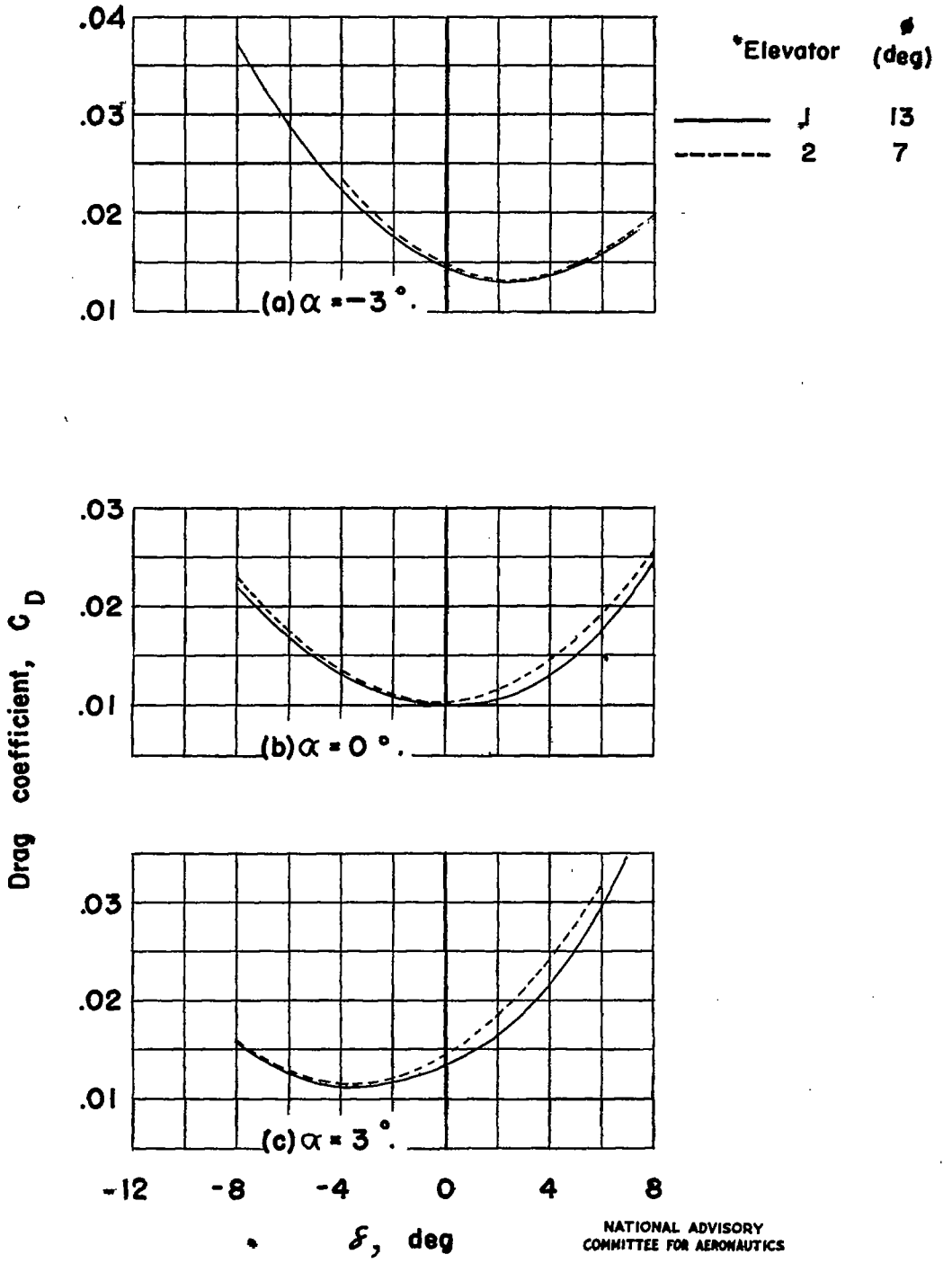

Figure 12.— Effect of elevator trailing-edge angle on drag coefficient. M = 0.35.

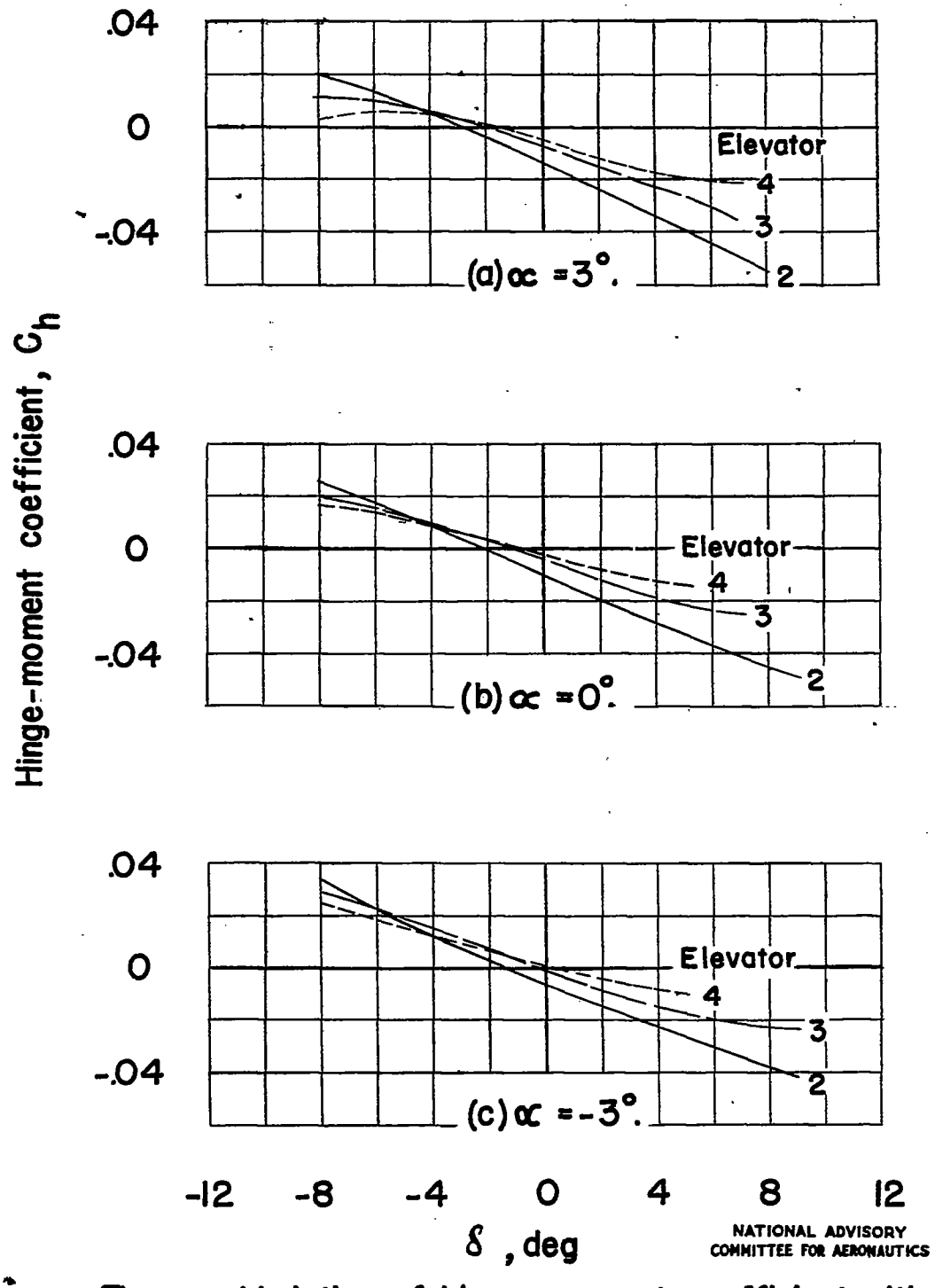

Figure 13.-Variation of hinge-moment coefficient with elevator angle for the three nose shapes. M = 0.35.

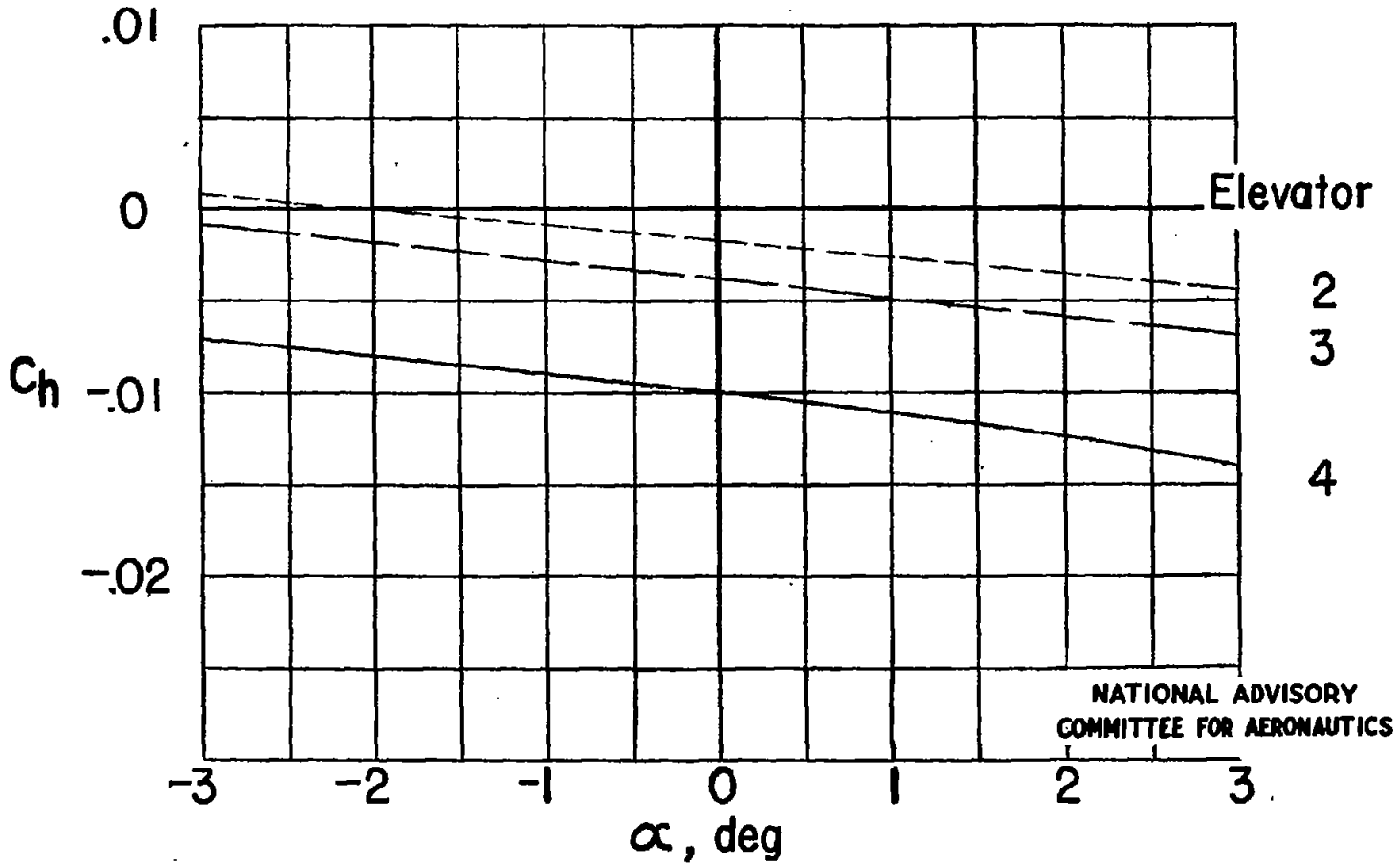

Figure 14 .— Effect of nose shape on hinge-moment coefficient. $\delta = 0°$; $M = 0.35$.

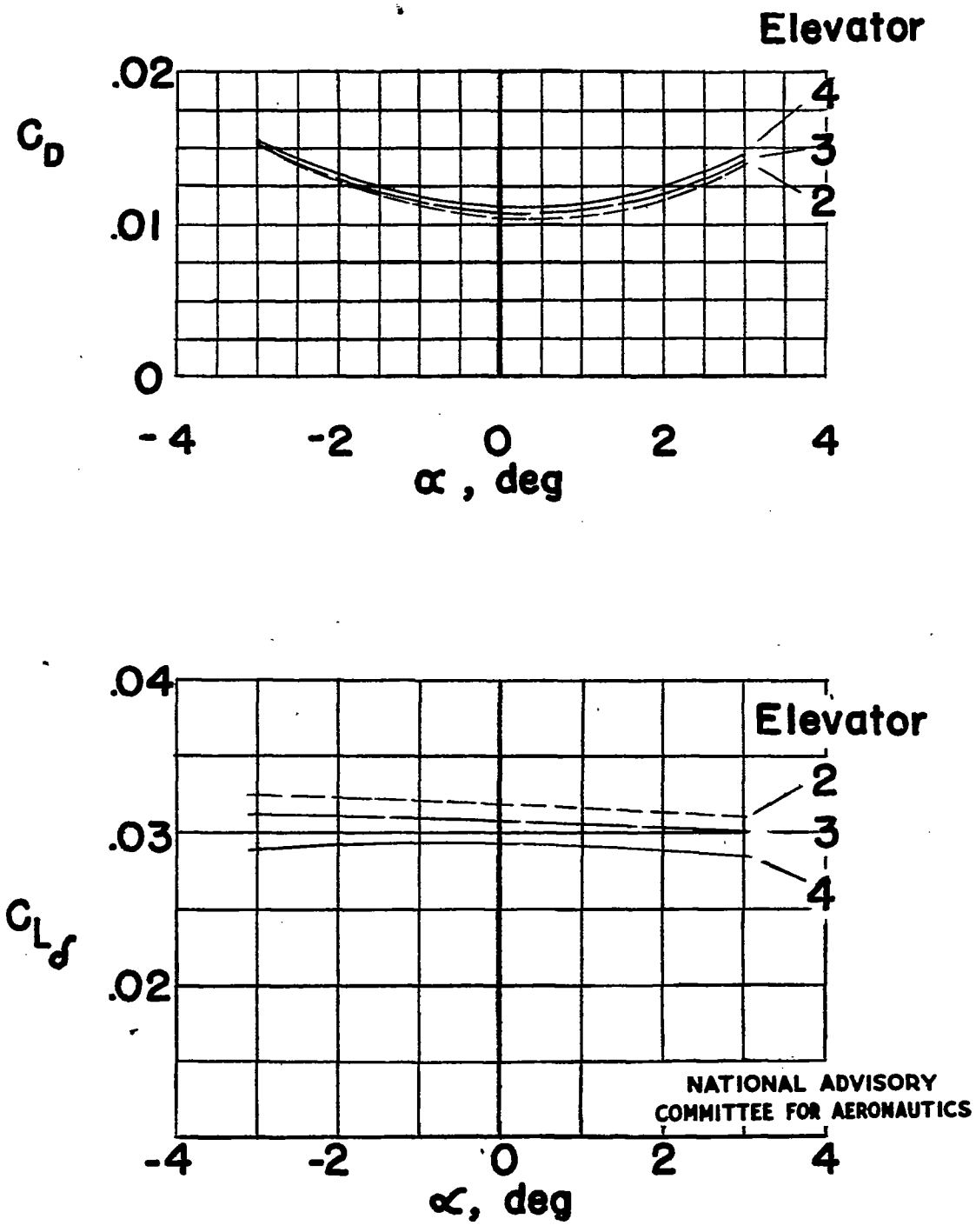

Figure 15.–Variation of C_D and C_{L_δ} with α for various nose shapes. $M = 0.35; \delta = 0°$.

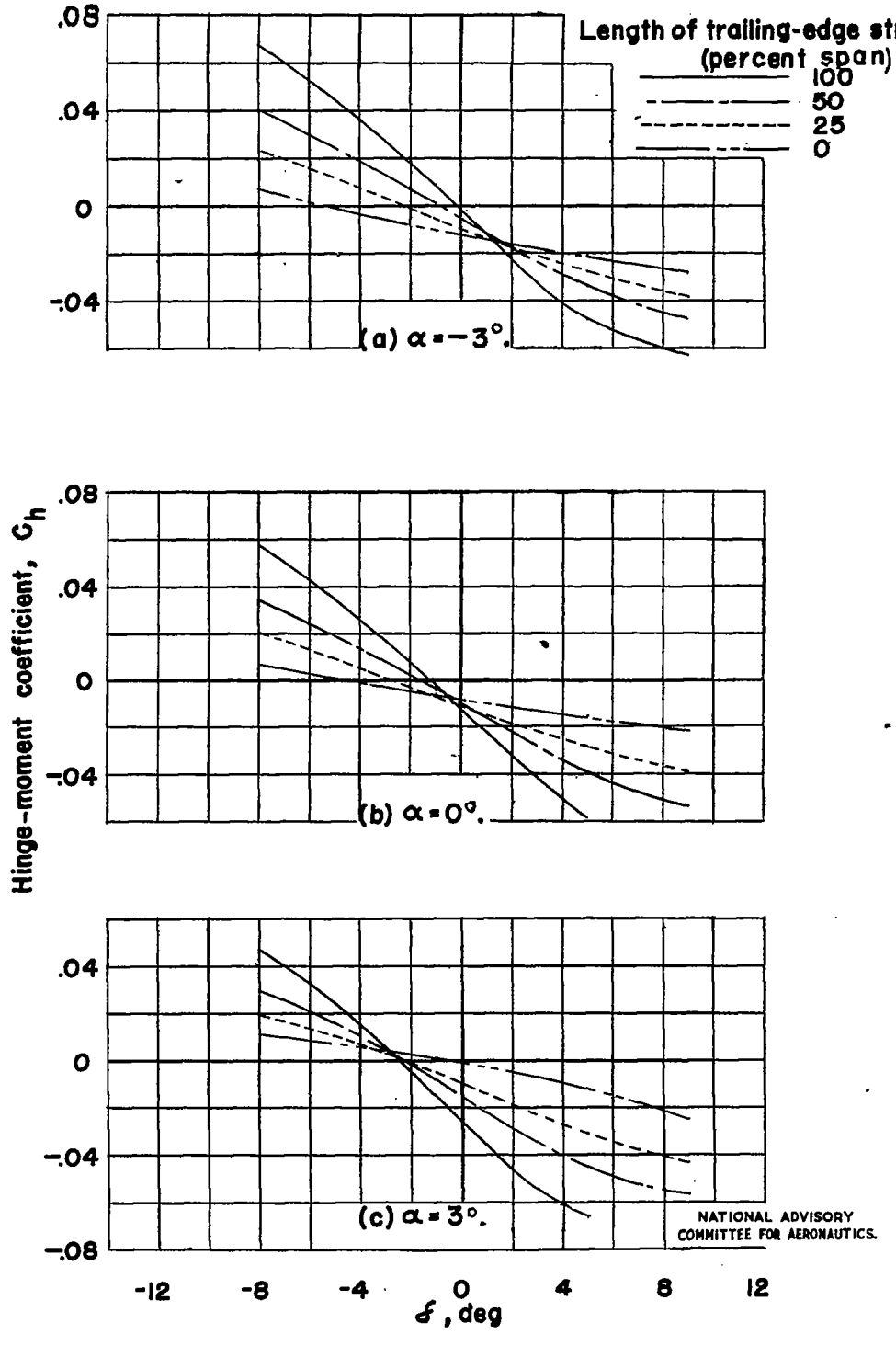

Figure 16.– Variation of C_h with elevator angle for four lengths of $\frac{1}{8}$-inch-diameter trailing-edge strips. M = 0.35.

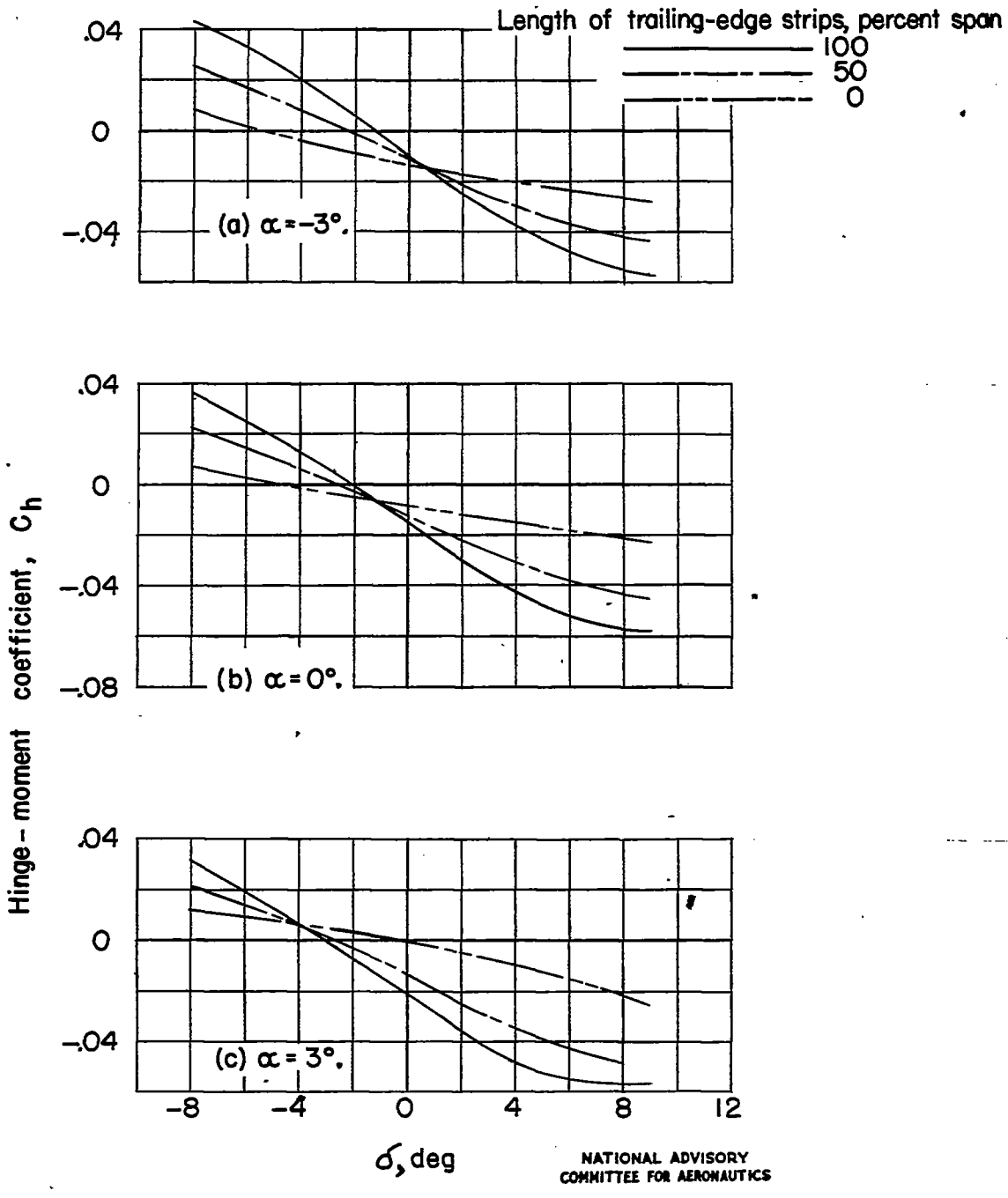

Figure 17.— Variation of C_h with elevator angle for three lengths of $\frac{1}{16}$-inch-diameter trailing-edge strips. M = 0.35.

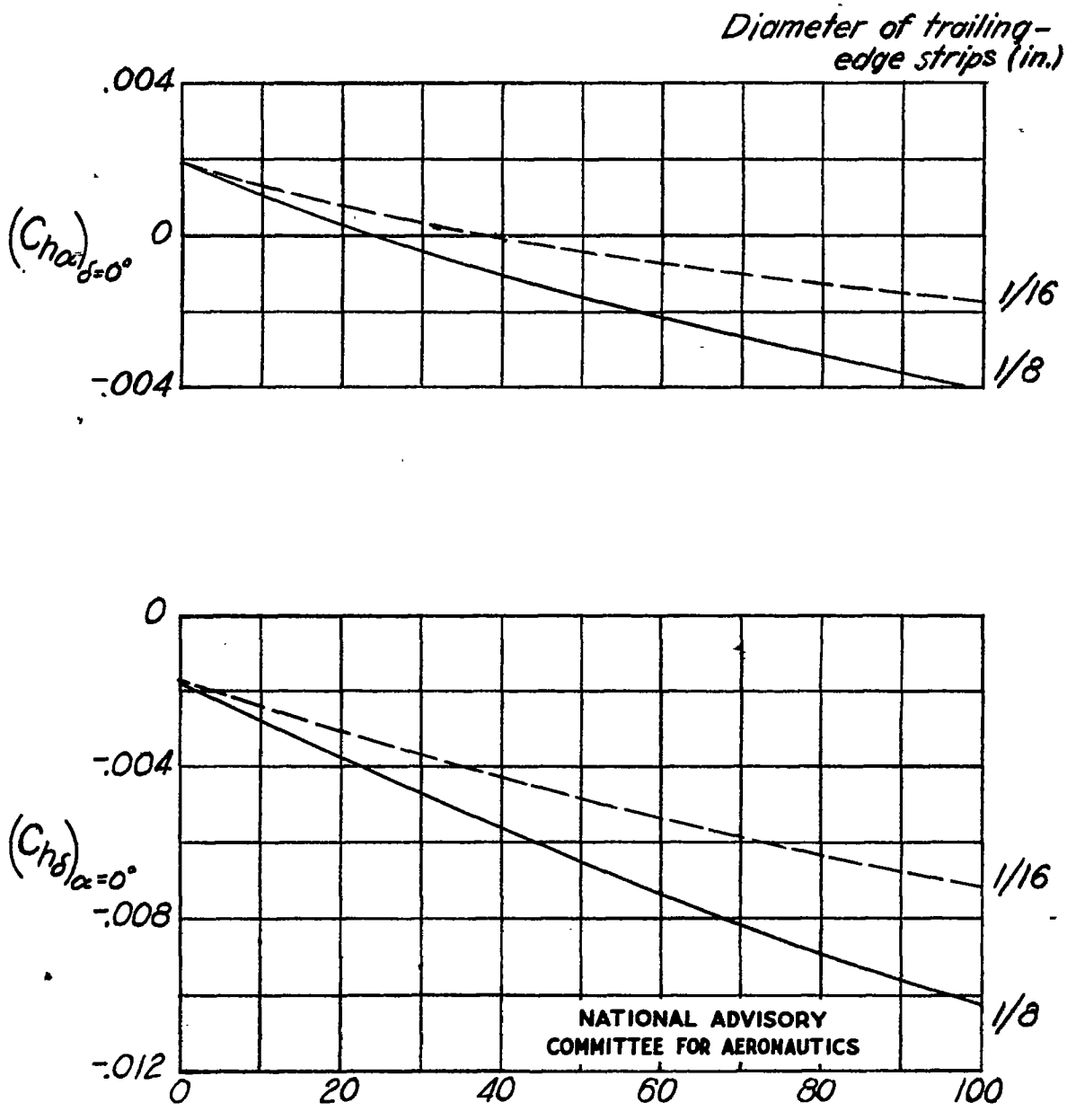

Figure 18.- Effect of length of trailing-edge strips of $\frac{1}{16}$-inch and $\frac{1}{8}$-inch diameter on C_{h_α} and C_{h_δ}. $M = 0.35$.

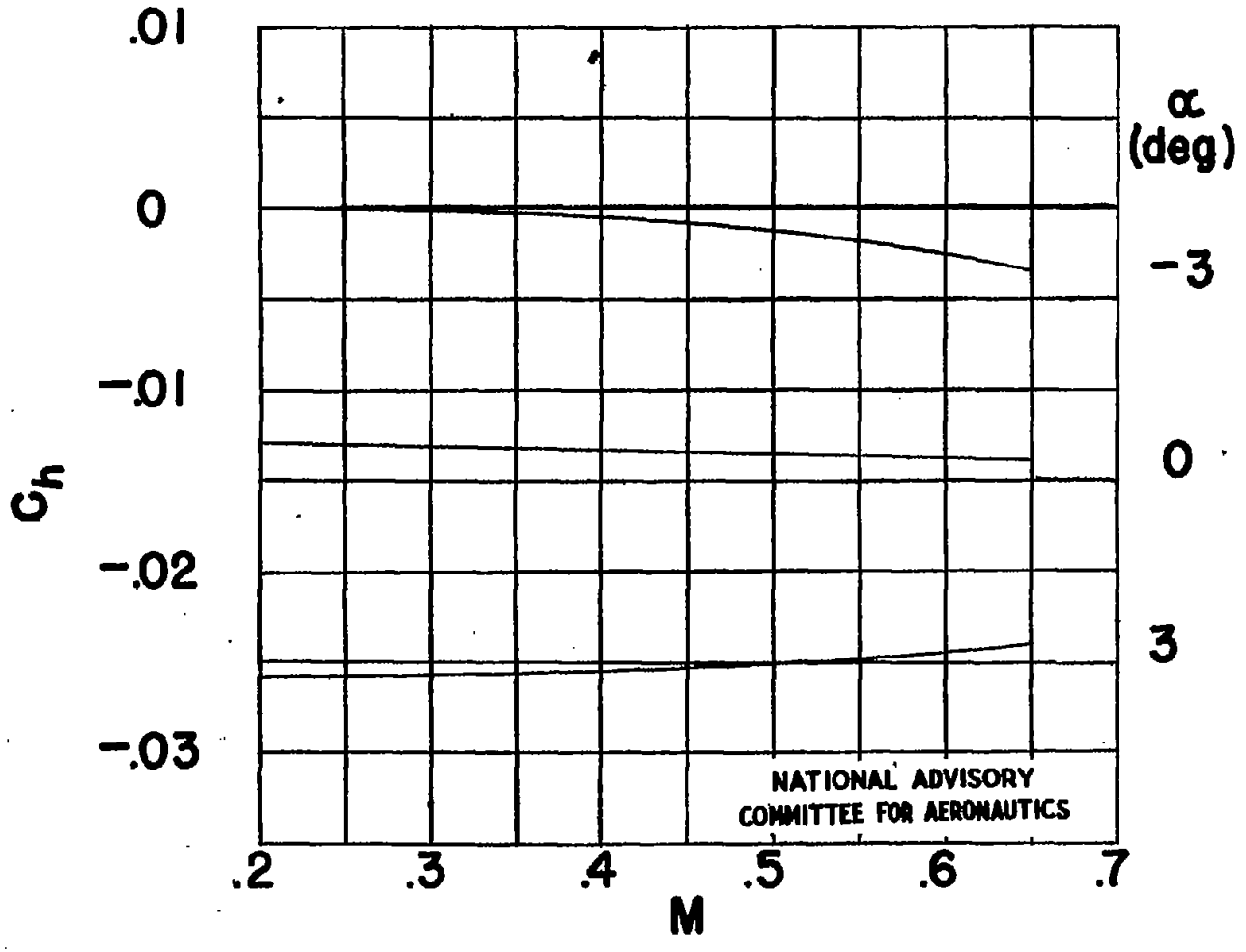

Figure 19.—Variation of elevator hinge-moment coefficient with Mach number for $\frac{1}{8}$-inch-diameter trailing-edge strips. Full span; $\delta = 0°$.

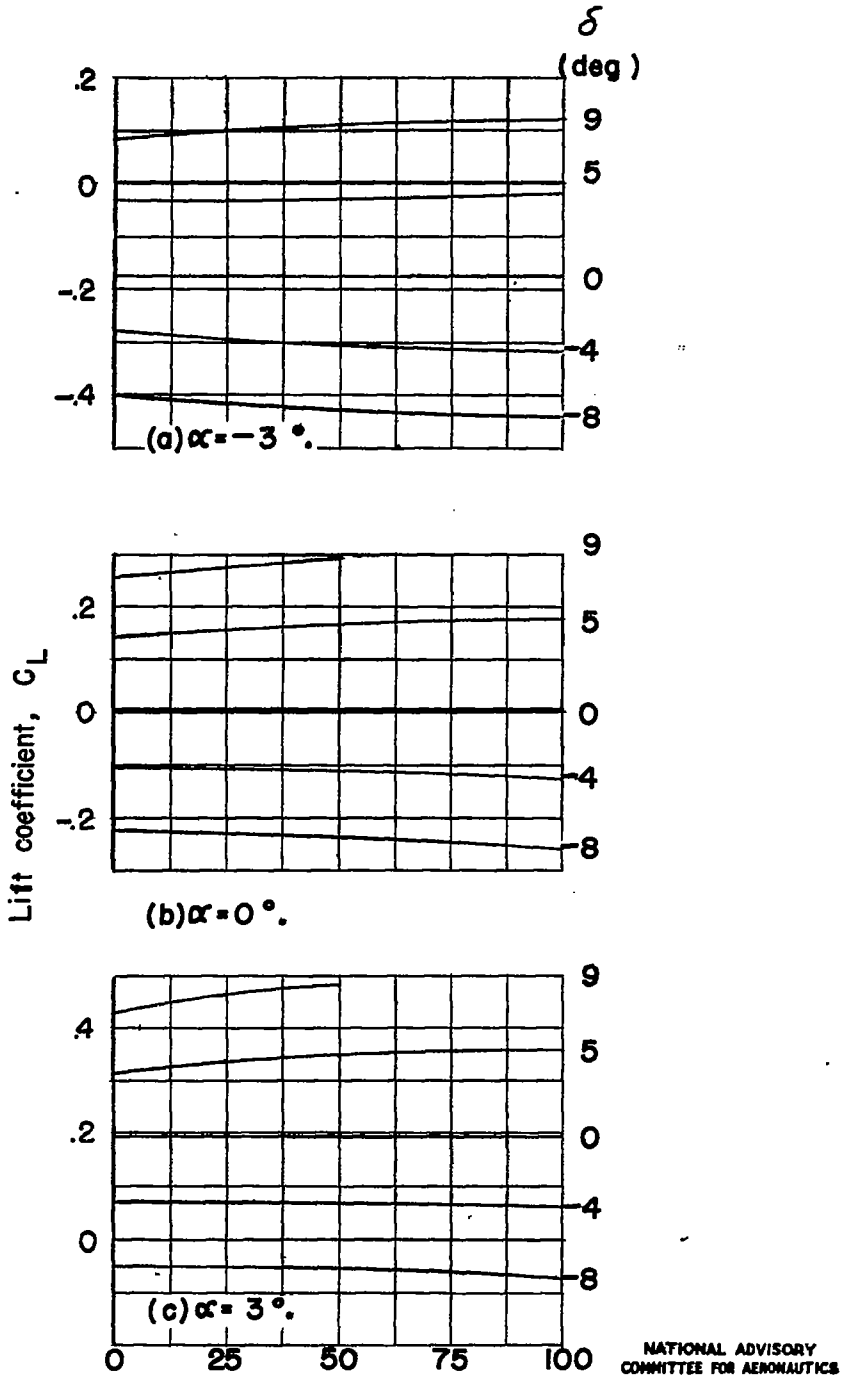

Figure 20.—Variation of lift coefficient with length of $\frac{1}{8}$-inch-diameter trailing-edge strips. M = 0.35.

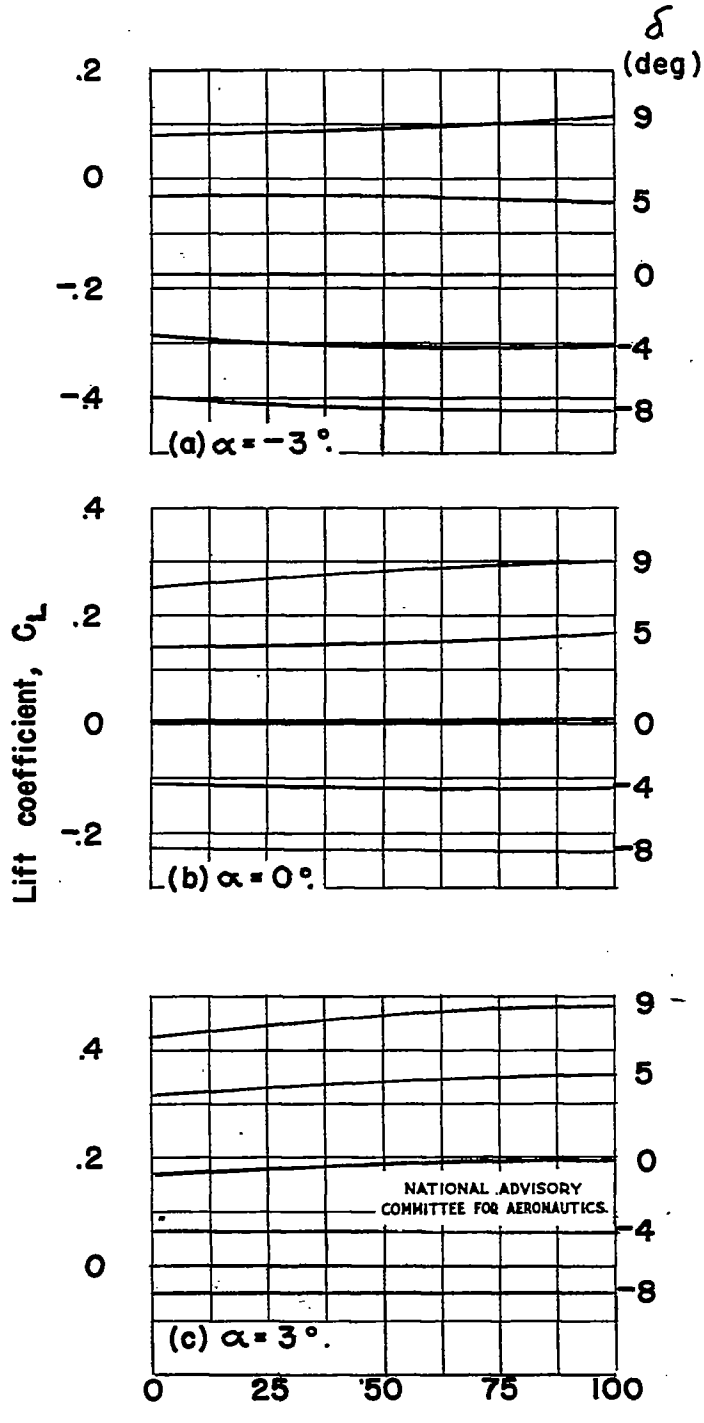

Figure 21.—Variation of lift coefficient with length of $\frac{1}{16}$-inch-diameter trailing-edge strips. M = 0.35.

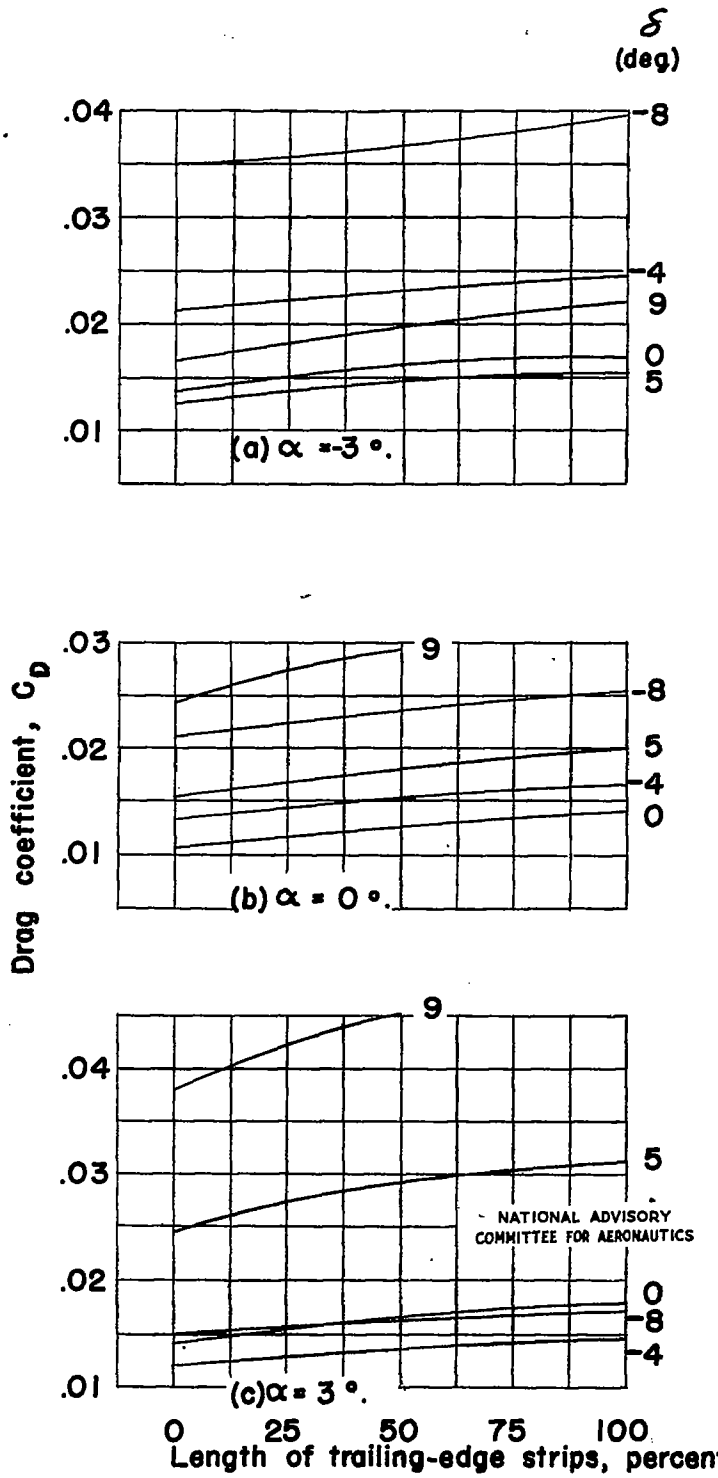

Figure 22.—Variation of drag coefficient with length of $\frac{1}{8}$-inch-diameter trailing-edge strips. M = 0.35.

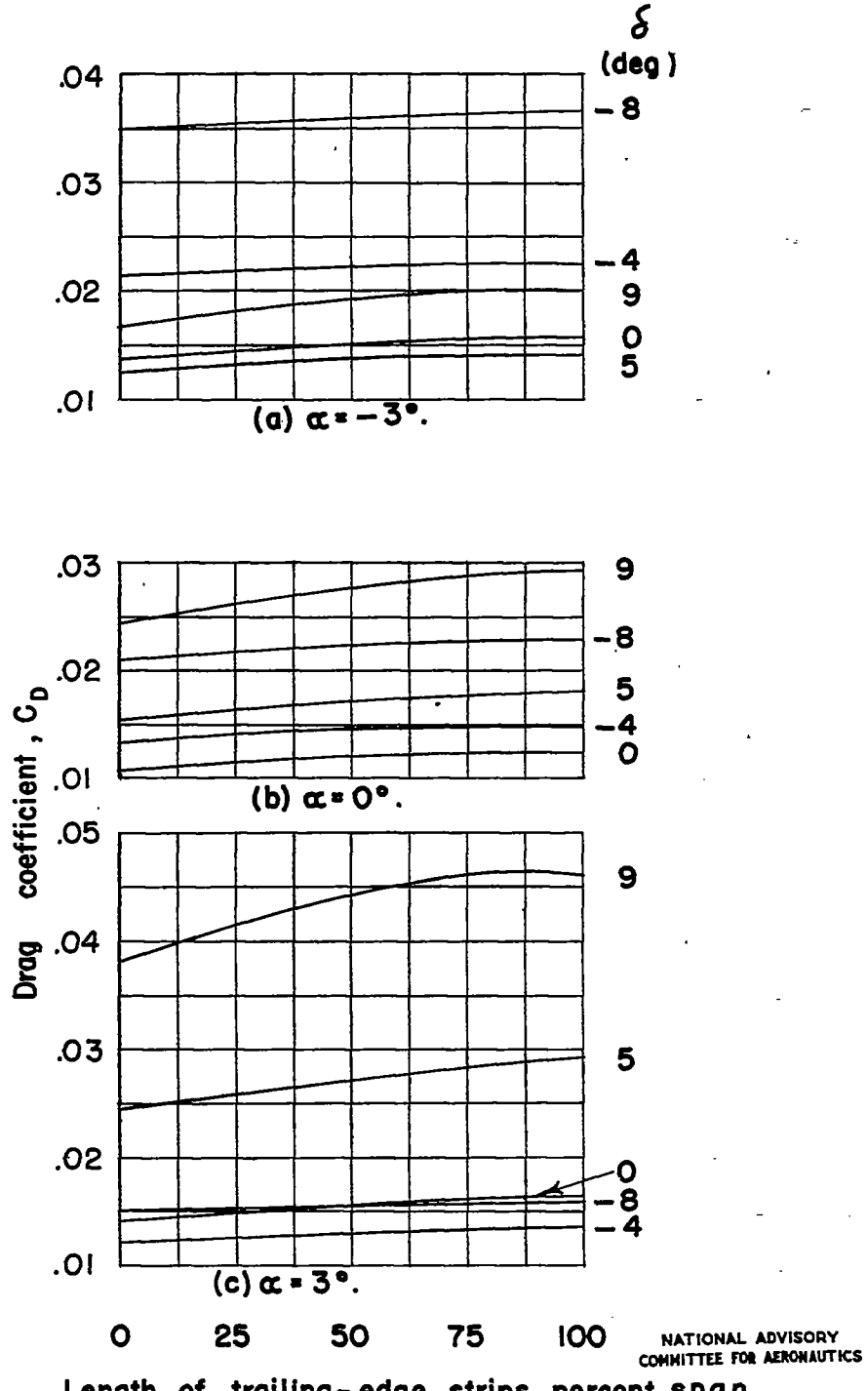

Figure 23.—Variation of drag coefficient with length of $\frac{1}{16}$-inch-diameter trailing-edge strips. M = 0.35.

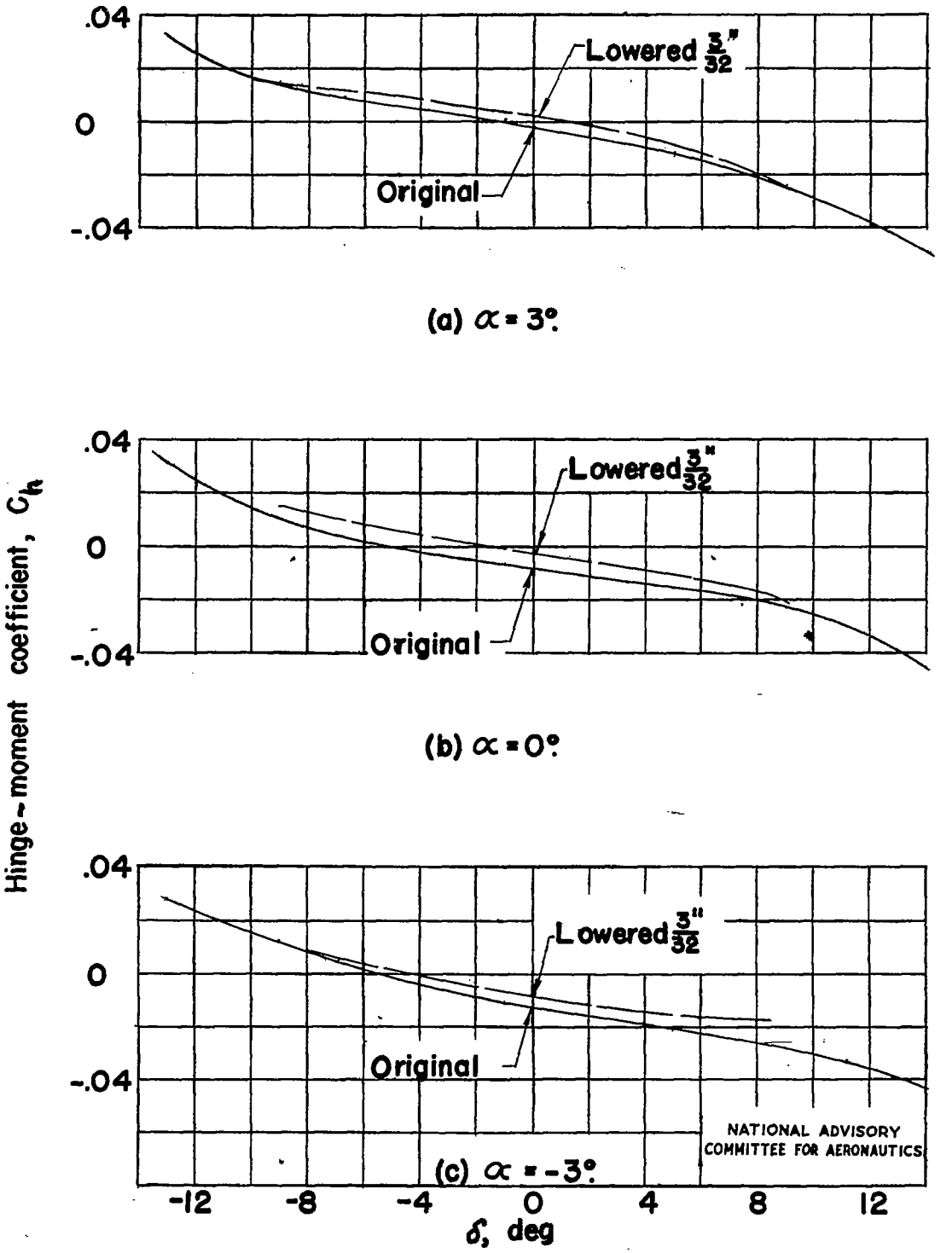

Figure 24.——Variation of hinge-moment coefficient with elevator angle for the two hinge positions. Metal elevator; M = 0.35.

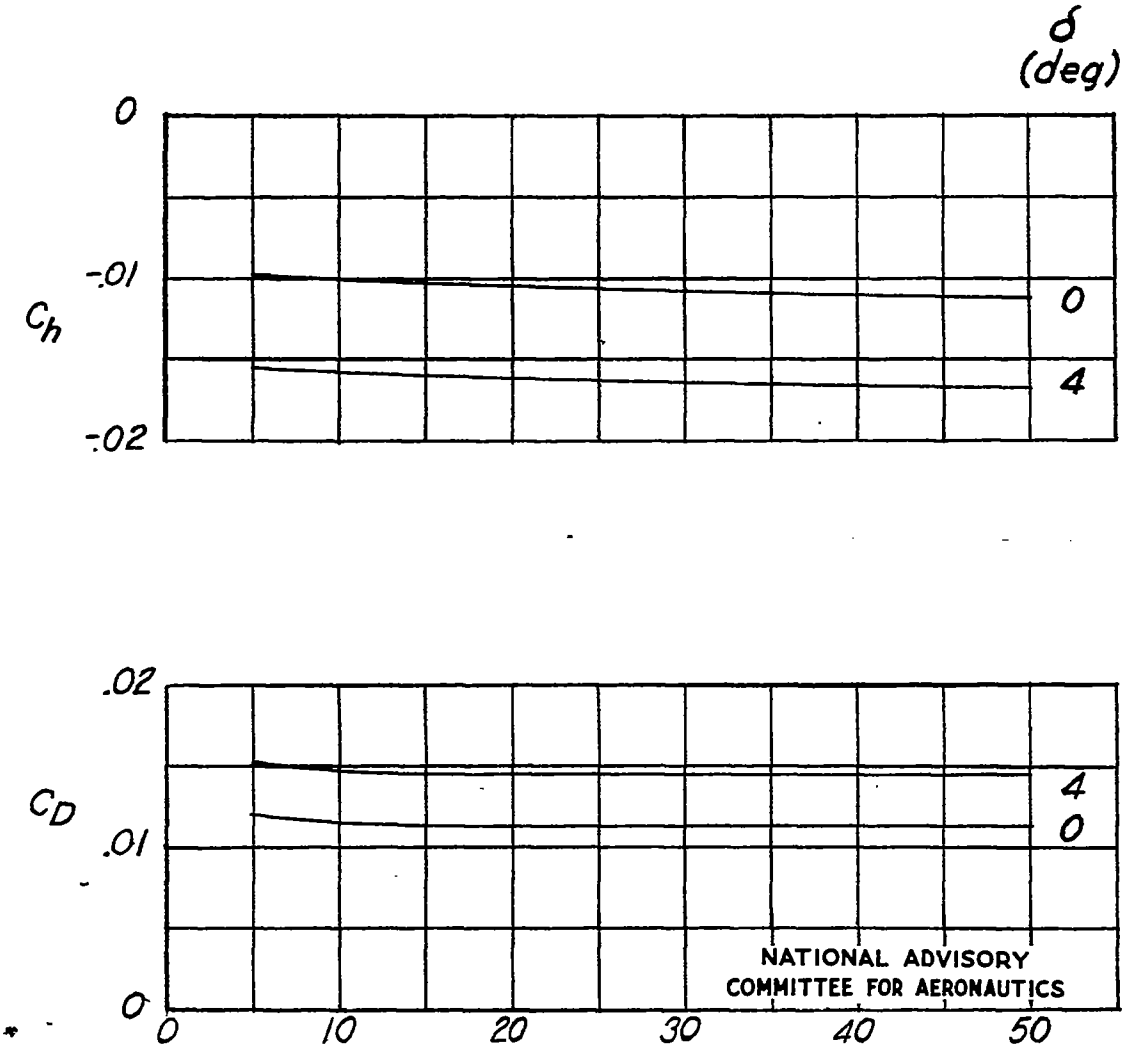

Figure 25.- Variation of drag and hinge-moment coefficents with location of transition strip, upper surface. $M=0.45$; $\alpha=0°$. Metal elevator.

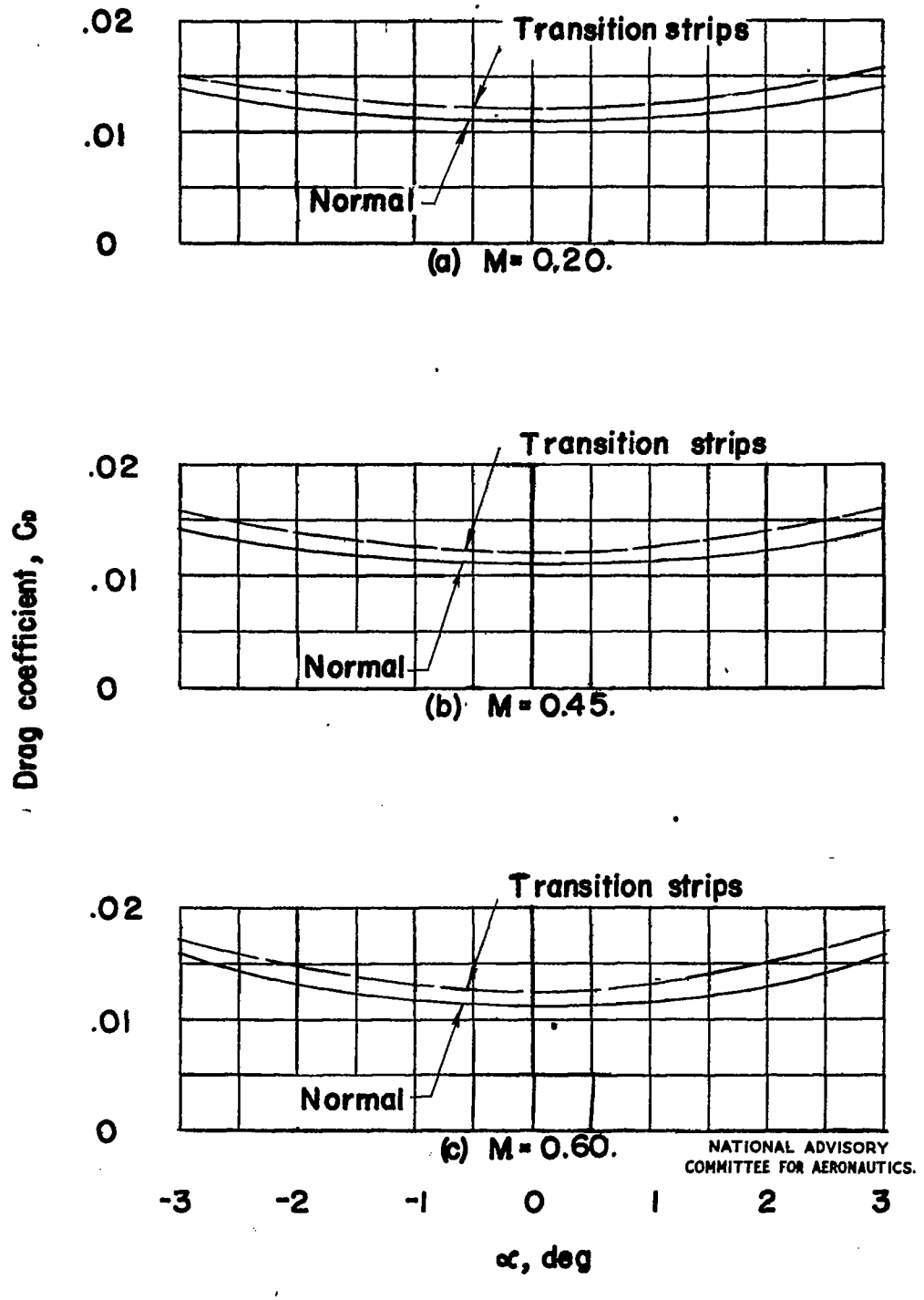

Figure 26.-Variation of drag coefficient with angle of attack for the normal condition and with transition strips at 5 percent chord. δ = 0°; metal elevator.

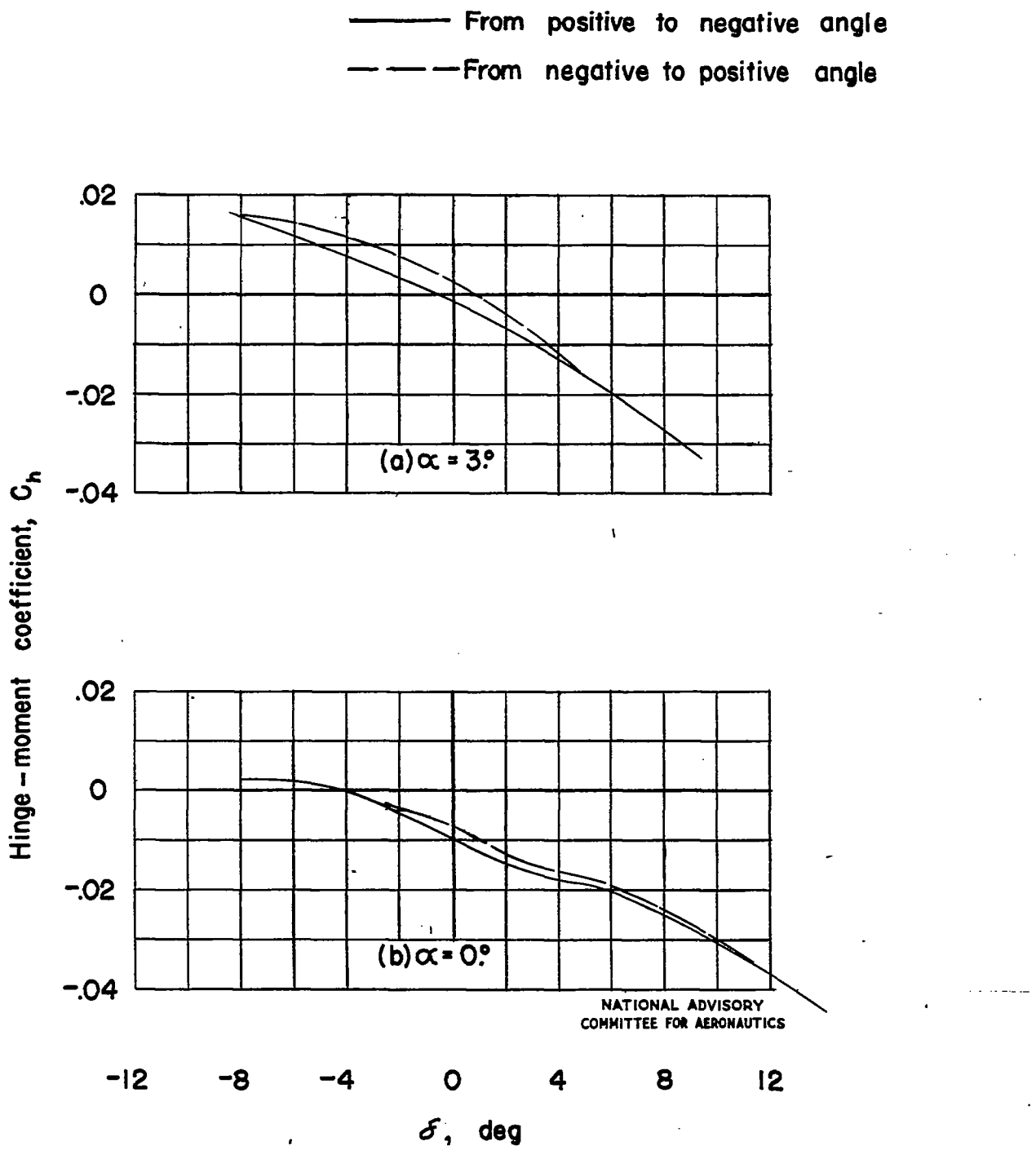

Figure 27.— Effect of aerodynamic hysteresis on hinge-moment coefficient. Metal-covered elevator; M = 0.50.

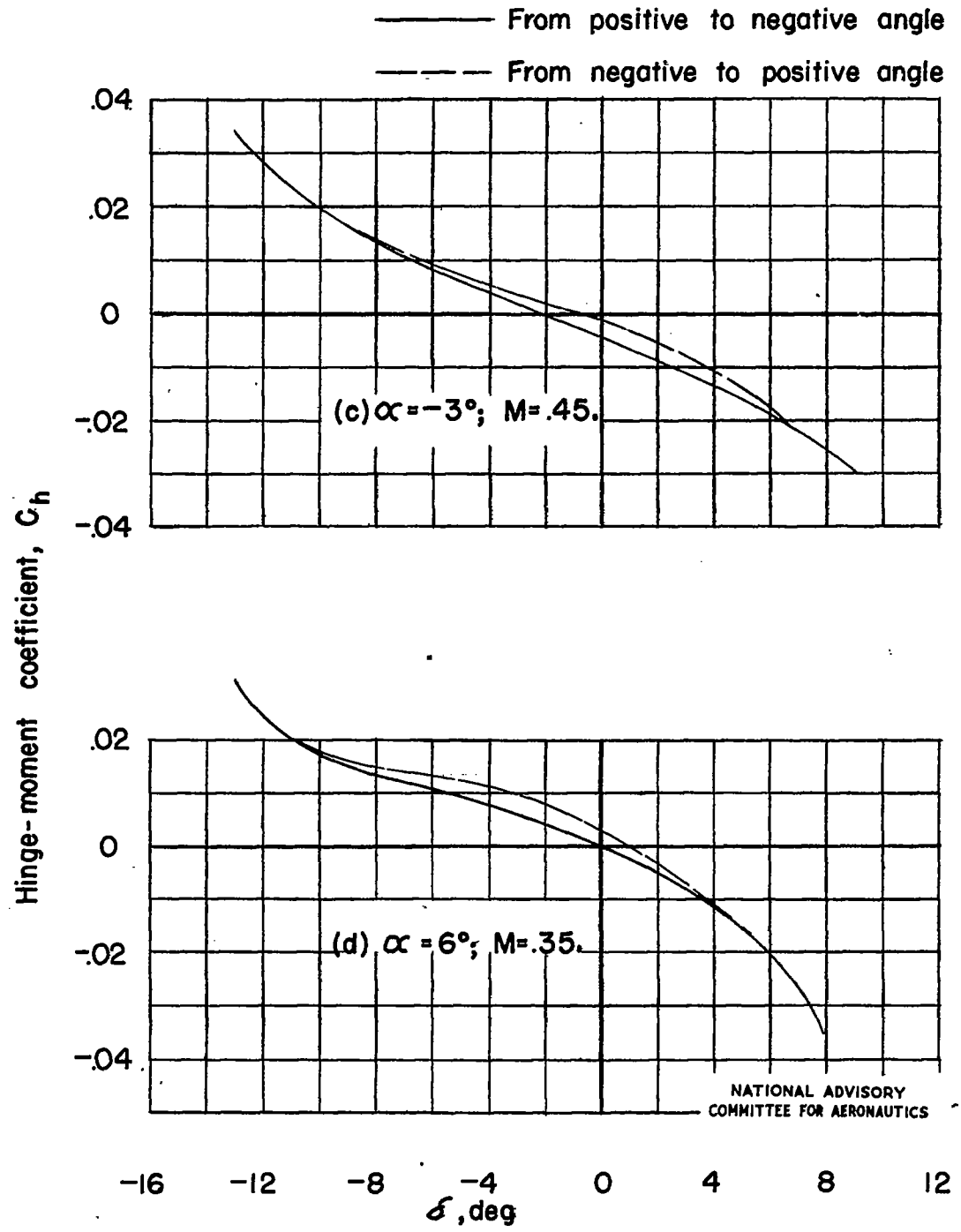

Figure 27.— Concluded.

Fig. 28

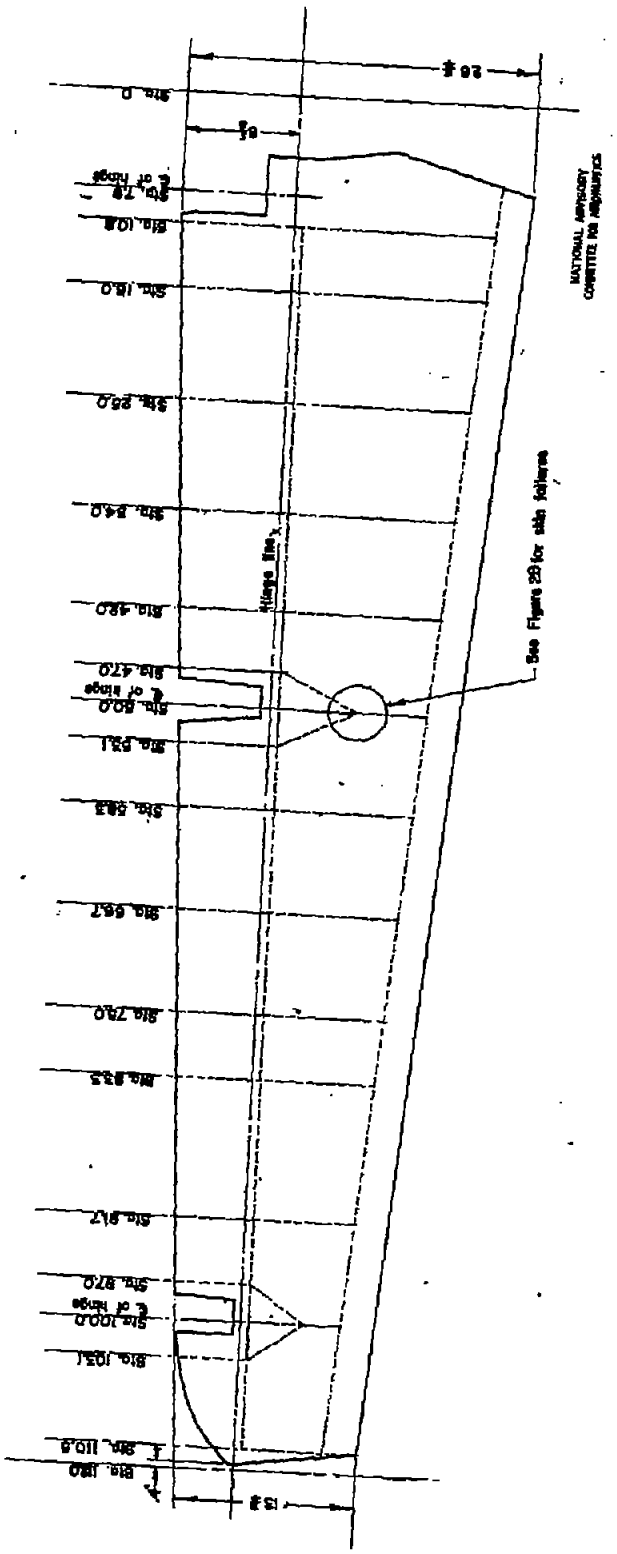

Figure 28.—Detail of metal-covered elevator. All dimensions are in inches.

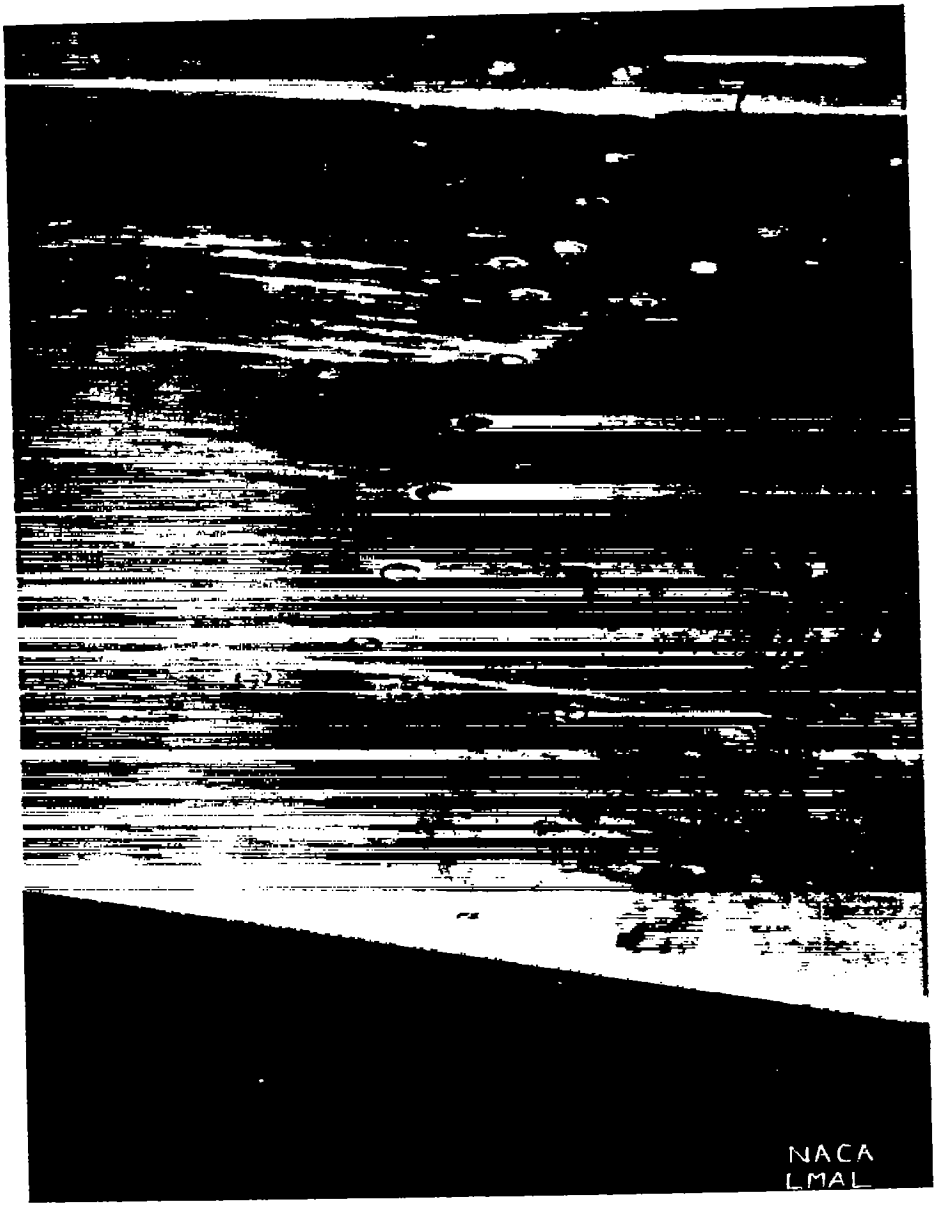

Figure 29.- Detail of upper-surface skin failure at station 50.

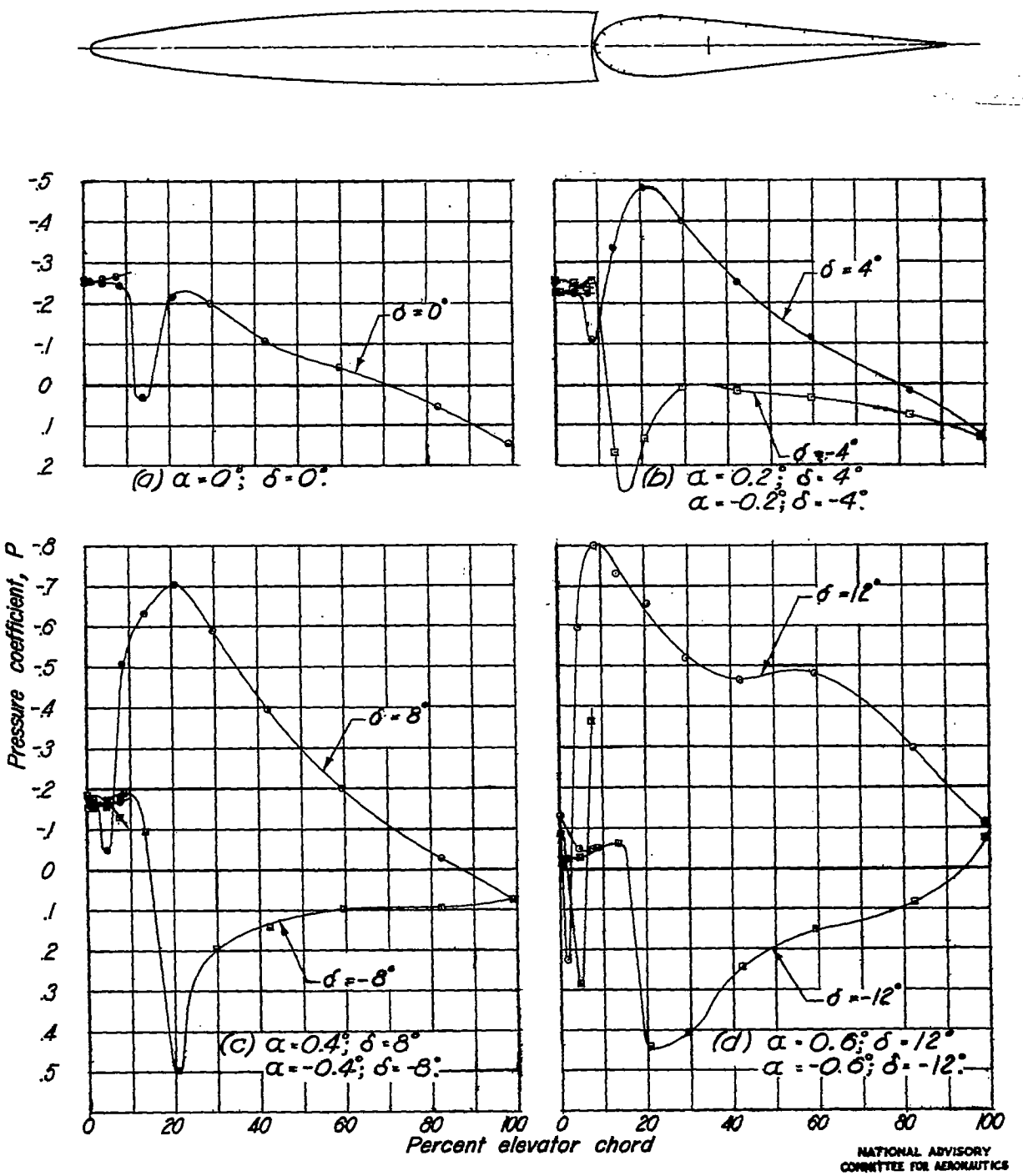

Figure 30.– Pressure distributions over the metal elevator at M = 0.20.

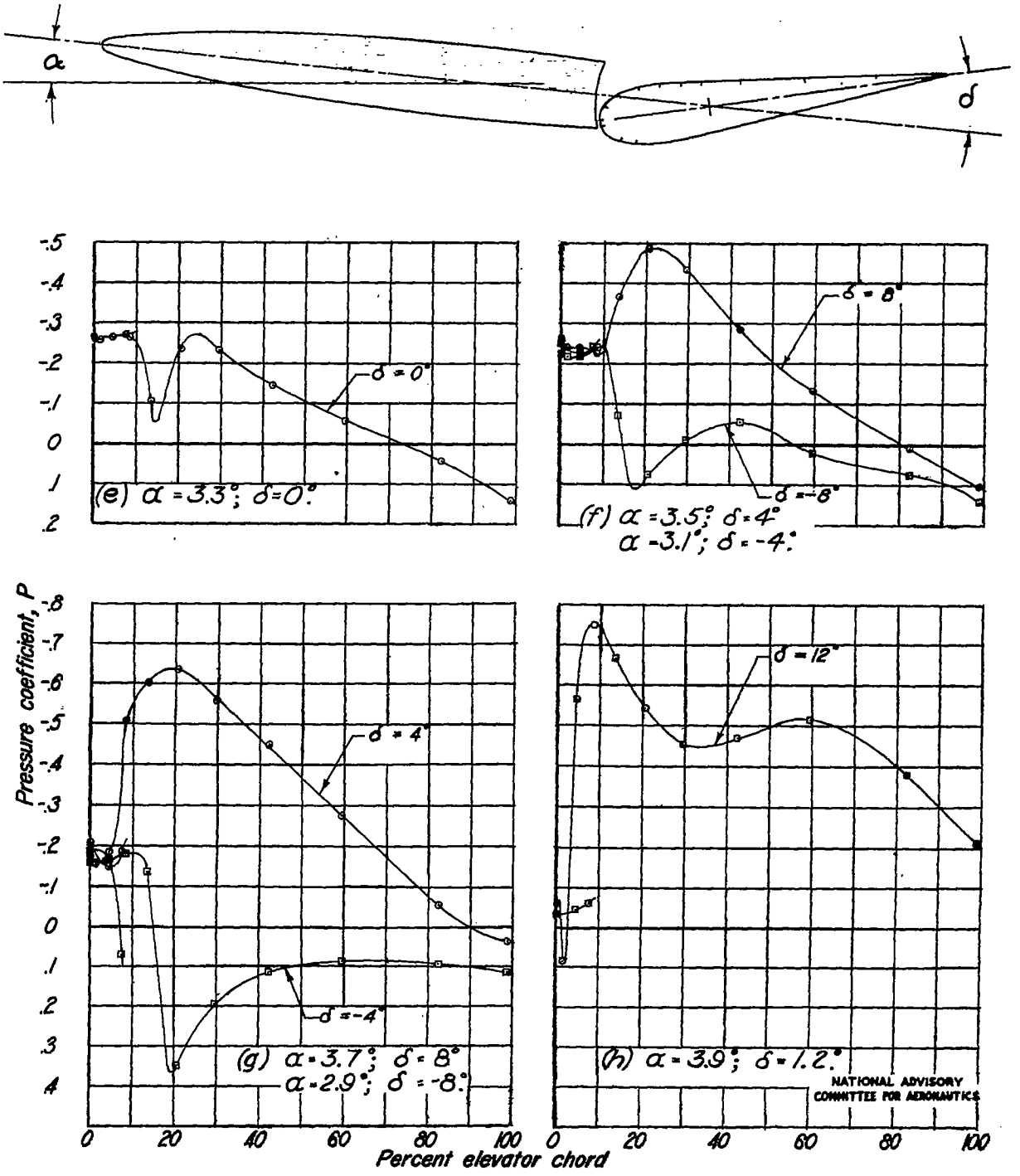

Figure 30.- Concluded.

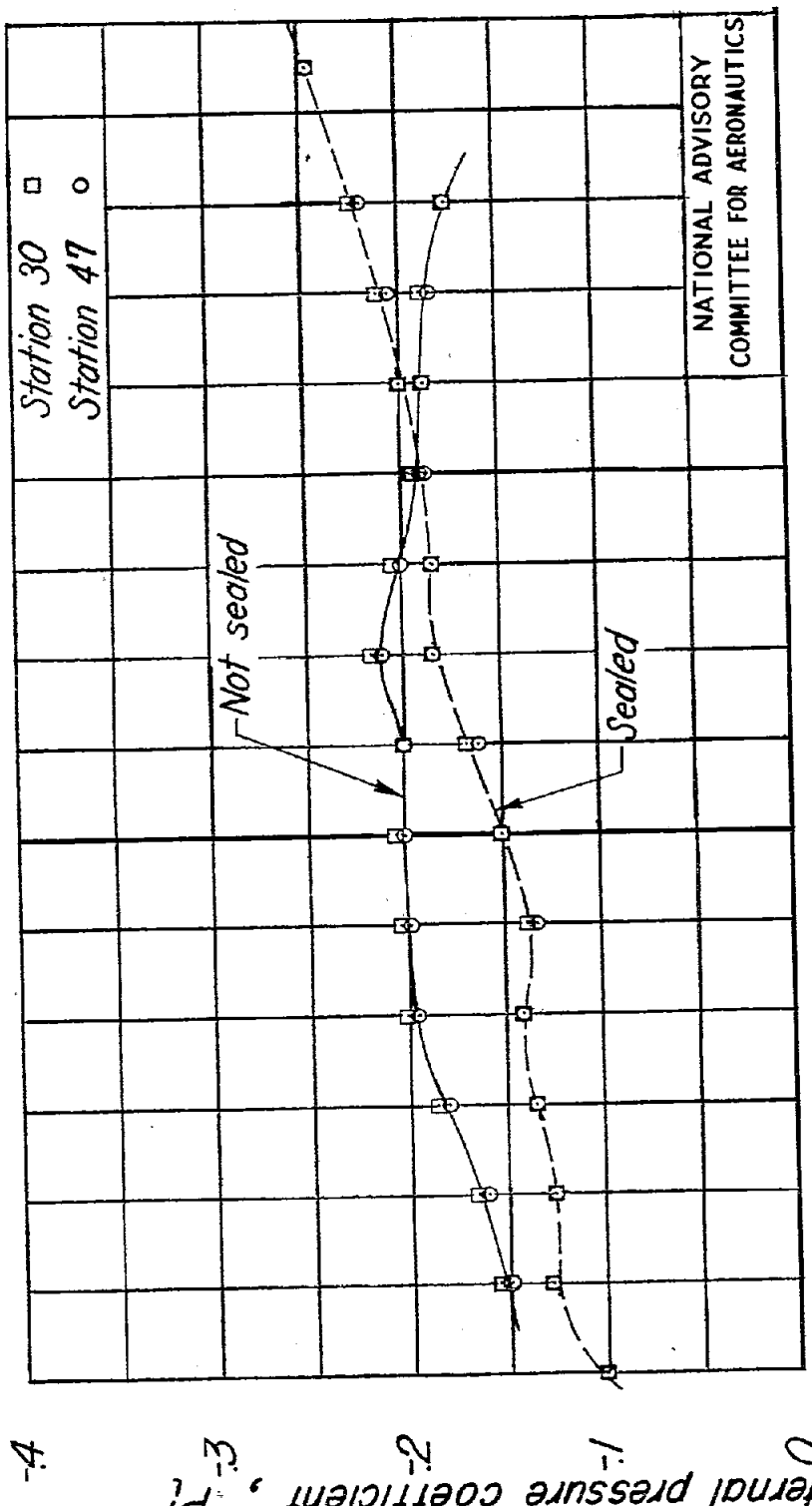

Figure 31.- Variation of internal pressure coefficient with elevator angle. $\alpha = 0°$; $M = .20$.